Resources, Conservation & Recycling 197 (2023) 107096

Contents lists available at ScienceDirect

Resources, Conservation & Recycling

journal homepage: www.elsevier.com/locate/resconrec

Full length article

Development of sustainable low carbon Engineered Cementitious Composites with waste polyethylene fiber, sisal fiber and carbonation curing

WeiHsiu Hu [a], Duo Zhang [b], Esayas Ftwi [c], Brian R. Ellis [a], Victor C. Li [a,*]

[a] Department of Civil and Environmental Engineering, University of Michigan, Ann Arbor, MI, United States
[b] State key laboratory of water resources and hydropower engineering science, Wuhan University, Wuhan, China
[c] School of Civil and Environmental Engineering, Addis Ababa University, Addis Ababa, Ethiopia

ARTICLE INFO

Keywords:
Engineered cementitious composites (ECC)
Carbonation curing
CO_2 sequestration
Sisal fiber
CO_2 footprint
Waste polyethylene fiber

ABSTRACT

Engineered cementitious composites (ECC) is an advanced fiber-reinforced cementitious composite with high tensile ductility. However, the binder and fiber system in ECC incur high economic and environmental cost. In this study, a low carbon ECC was developed by substituting virgin polyethylene fiber with waste polyethylene fiber (WPE) from waste marine fishing nets. Carbonation curing was applied to further reduce embodied carbon footprint via direct CO_2 mineralization. This research examined the low carbon ECC's mechanical properties, including compressive strength and tensile strength and ductility. The CO_2 footprint and material costs of ECC were also investigated. The objective was to develop an ECC competitive to normal concrete economically and environmentally while maintain the unique ductile performance of ECC. Results suggest that carbonation-cured WPE reinforced ECC possesses 50% of the CO_2 footprint and 37% of the cost of traditional concrete. Meanwhile, this low carbon ECC maintains at least 4 MPa tensile strength and 6% tensile ductility. This research demonstrates the feasibility of developing construction materials with low environmental impact while maintaining high performance for civil infrastructure applications. The adoption of WPE in ECC provides a plausible pathway to recycle marine waste into the construction industry that urgently needs to be decarbonized.

1. Introduction

Ocean plastic pollution has become a major environmental challenge (Ritchie and Roser, 2018). The annual marine plastic debris that flows into ocean are expected to be 9–23 million tons and will continuously increase without any action (Borrelle et al., 2020; The PEW Charitable Trusts and SystemIQ, 2020). Specifically, abandoned, lost and discarded fishing gear (ALDFG) is recognized as the most harmful waste of marine plastic pollution, which enters ocean 1.9–2.3 million tons annually (Borrelle et al., 2020; Global Ghost Gear Initiative, 2022). The ALDFG seriously impacts aquatic ecosystem and threatens fish stocks, causing approximately 3300–33,000 USD per tons economic costs annually (Beaumont et al., 2019). It requires a significant reduction in plastic debris to solve this crisis by recycling the gear that is recovered or at end of life in accordance with the Global Ghost Gear Initiative (GGGI) (Global Ghost Gear Initiative, 2022) and find alternative applications for the recycled plastic waste materials.

Mitigating CO_2 emissions is one of the most critical challenges for our society. If all countries in the world meet their current targets set within the Paris climate agreement, the estimated warming will be around 2.6–3.2 ° Celsius in 2100 (Ritchie et al., 2020). The production of Portland cement accounts for 8% of global CO_2 emissions, which makes concrete a significant CO_2 emitter (Ritchie et al., 2020). As the global construction market continuously expands, effective strategies for mitigating concrete CO_2 footprint are much needed (Hasan et al., 2023). Repurposing the waste ALDFG, i.e., waste fishing nets into fibers for reinforcement of concrete may be a potential solution by substituting the conventional synthetic fiber with the recycled waste fishing nets. Nguyen et al. (2021) pioneered the study of concrete reinforcement with fibers from waste fishing nets.

ECC is a fiber-reinforced cementitious composite that has high tensile ductility several hundred times that of normal concrete (Li, 2019). It has been proven that the intrinsic tight crack width of ECC even when highly strained retains a lower water permeability (Lepech and Li, 2009)

* Corresponding author.
E-mail address: vcli@umich.edu (V.C. Li).

https://doi.org/10.1016/j.resconrec.2023.107096
Received 29 January 2023; Received in revised form 7 June 2023; Accepted 16 June 2023
Available online 27 June 2023

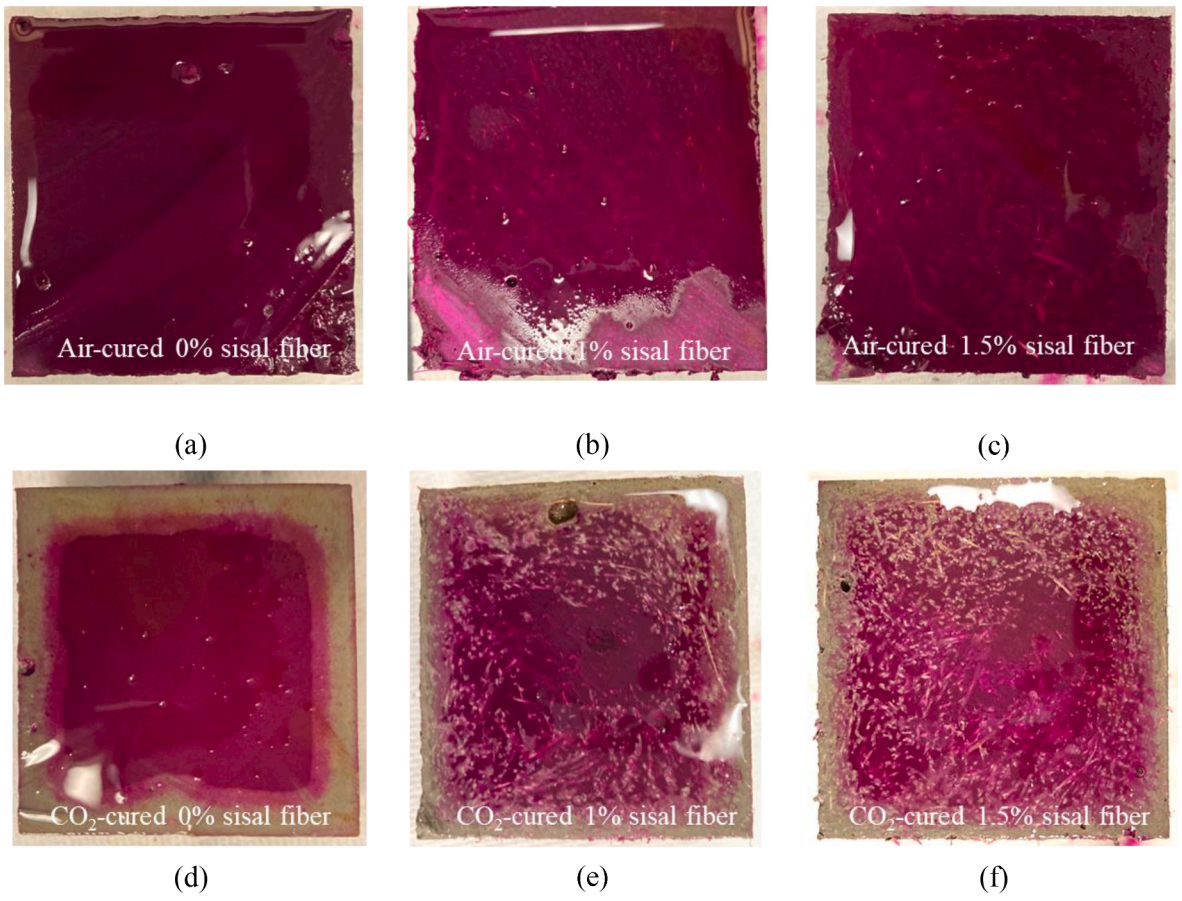

Fig. 1. Carbonation depths and patterns as revealed by the phenolphthalein indicator, for air-cured (a) 0% sisal fiber, (b) 1% sisal fiber, (c) 1.5% sisal fiber; and carbonation-cured (d) 0% sisal fiber, (e) 1% sisal fiber, (f) 1.5% sisal fiber ECC.

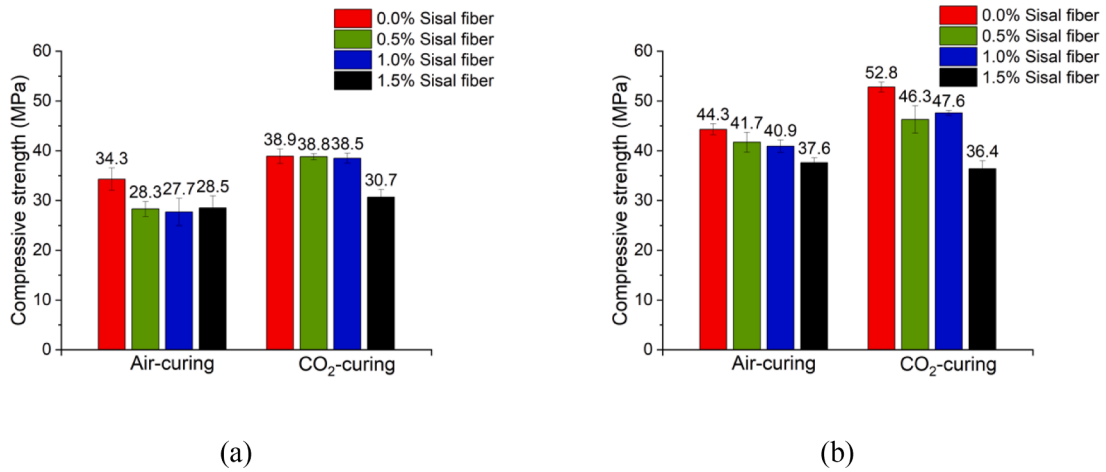

Fig. 2. Compressive strength for 2% WPE OPC-ECC at (a) 7 days, and (b) 28 days.

and chloride diffusivity (Sahmaran et al., 2007), leading to enhanced infrastructure durability (Lepech et al., 2008). This implies the feasibility of developing low maintenance civil infrastructure with low operational carbon. ECC is now deployed in the building, transportation, and energy infrastructures for enhanced resilience and durability (Li, 2019).

Despite the advantages, the high amount of cement in ECC due to eliminating the coarse aggregate led to a high embodied CO_2 footprint for ECC. For example, M45 ECC, a most studied ECC mix composition, possesses an embodied carbon footprint twice that of conventional concrete (Shoji et al., 2022). The development of a truly low-carbon ECC remains an open challenge. In recent research, industrial waste materials (IWMs) were used as substitutes for raw materials (Othman et al., 2023) in typical ECC mixtures to reduce the CO_2 footprint of ECC (Bahraq et al., 2020) such as limestone calcined clay cement (LC3) ECC. LC3 improves the tensile ductility and crack width control capacity of ECC (Yu et al., 2020; Zhang et al., 2020a; Zhu et al., 2020), reduce the cement carbon emissions and costs by up to 35% (Sánchez Berriel et al., 2016) and 15–25% (Cancio Díaz et al., 2017) compared to ordinary Portland cement (OPC), although the compressive strength of LC3-ECC

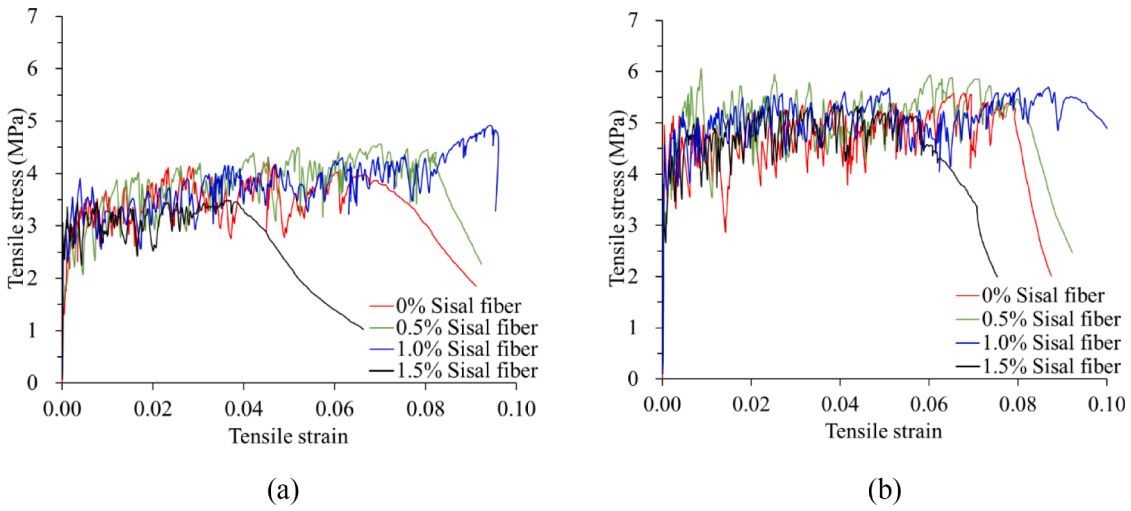

Fig. 3. Representative tensile stress-strain relationship for 2% WPE (a) air-cured, (b) CO_2-cured OPC-ECC at 7 days.

Table 1
The embodied energy, carbon emission, and material cost for ingredients ECC production.

Component	Embodied energy (GJ/t)	CO_2 emission (kg/t)	Cost (USD/t)
OPC type 1	4.8–5.5[a]	870–940[b]	48[c]
LC3[c]	4	550	40.3
FA	0	0	25.6[c]
Silica sand[c]	0.067	23.3	63.9
WR[c]	35	1667	1211
Conventional PE fiber	73–116[d]	2000[d]	35,200[e]
Sisal fiber	18[f]	170[f]	682

[a] Data from (Marceau et al., 2006).
[b] Data from (Damtoft et al., 2008; Pacheco-Torgal et al., 2017).
[c] Data from (Wu et al., 2018; Zhang et al., 2020a; Zhu et al., 2020), where CO_2 emission of LC3 can also be presented in 1344–1562 kg/m^3.
[d] Data from (Shoji et al., 2022; Zhang et al., 2020c).
[e] Data from (Fu et al., 2022).
[f] Data from (Broeren et al., 2017).

is lowered by 12–30% compared to OPC-ECC (Zhu et al., 2020). By substituting OPC with LC3, ECC's CO_2 footprint and costs can be significantly reduced (Shoji et al., 2022).

Polyvinyl alcohol (PVA), polypropylene (PP), and polyethylene (PE) fibers are common fibers for reinforcing ECC. Specifically, PVA fiber has been tailored with a surface coating for optimal reinforcement performance in ECC (Li et al., 2002). PE fiber has been widely applied to high-performance ECC due to its high strength, high aspect ratio, and high complimentary energy for multiple steady-state cracking, which positively affects ECC's performance (Zhou et al., 2020; Yu et al., 2019, 2018). However, PVA and PE fibers have high embodied carbon footprint, energy, and costs while PP fibers have limited reinforcement performance (Wan Ibrahim et al., 2014; Zhang et al., 2020c). It Is essential to find a substitute fiber for PVA and PE fibers that lowers the costs and carbon footprint of ECC to make it more competitive to conventional concrete. Waste polyethylene rope fiber (WPE) is an industrial waste fiber from the fishing industry, i.e., fishing nets. The waste fishing nets discard each year is about 10% of global marine plastic waste (by volume) (Macfadyen et al., 2009; Maria et al., 2016). Repurposing WPE for ECC has the potential to reduce marine waste while greening ECC. Specifically, WPE meets all the requirements for fiber in ECC: a minimum tensile strength of 1000 MPa, an inelastic failure strain greater than 5%, and a suitable diameter between 30 and 50 μm (Li et al., 2001), making it a potential substitute fiber for virgin PE or PVA fibers in low-carbon ECC.

Carbonation curing lowers concrete carbon footprint by sequestering CO_2 through its early-age curing process. During carbonation curing of a precast element, CO_2 reacts with calcium silicates and their hydration products and is converted into calcium carbonate ($CaCO_3$) (Zhang et al., 2021). Meanwhile, Rostami et al. (2012), Hu et al. (2023), Zhang et al. (2021, 2020b) studied the carbonation curing effect on the tensile, flexural, and fatigue performance of ECC which were found to be improved due to the accelerated cement reaction and denser microstructure by $CaCO_3$ precipitation. This also enhanced the fiber/matrix interface bonding to control crack width, which lowered the water permeability and promoted the self-healing of ECC (Lepech and Li, 2009; Li and Herbert, 2013). However, denser microstructure also limited CO_2 sequestration since it became harder for CO_2 to diffuse into the inner matrix. Therefore, finding a way to help CO_2 sequestrate deeper into a precast product is needed.

Sisal fiber has been used as a natural fiber reinforcement in cement and geopolymer composites (Ahmad et al., 2022; Hasanuddin et al., 2023; Tomas and Jose, 2022) for its low energy consumption and greenhouse gas emissions (Camargo et al., 2020). Sisal fiber is one of the most produced fibers globally and accounts for 2% of the world's plant fiber production with at least 300 thousand tons of annual production (Muthangya et al., 2009; Saxena et al., 2011). Compared to PE and glass fibers, sisal fiber lowers the embodied CO_2 footprint by 75–95% of and the embodied energy by 85–95% (Broeren et al., 2017). The geometry of sisal fiber is a tubular pillar (Wei, 2018; Wei and Meyer, 2014), which may serve as a conduit to promote CO_2 diffusion in a cementitious matrix, thus enhancing CO_2 sequestration. The reduced alkalinity by carbonation curing (Zhang and Shao, 2016) will also solve the well-known degradation problem of sisal fiber in a cementitious matrix (Camargo et al., 2020). In this study, sisal fibers were adopted for the sole purpose of channeling CO_2 deeper into the precast element, taking advantage of their hollow nature. Their mechanical reinforcement effect is assumed negligible when compared with that from the WPE fibers. Hence, any degradation of sisal fiber in an alkaline environment is unlikely to affect the composite's long-term properties.

By combining a low-carbon binder, CO_2 sequestration, and waste fiber utilization, this research develops a sustainable ECC with comparable cost and CO_2 footprint to conventional concrete while recycling the plastic marine waste. By using LC3, WPE, waste foundry sand (WFS), sisal fiber, and carbonation curing (see Appendix A, Fig. A1), a comprehensive experimental program including compressive strength, uniaxial tensile strength, crack patterns, interfacial bonding strength, cost, embodied carbon footprint and energy evaluation was initiated. To identify the effects of adding sisal fiber on ECC's mechanical properties

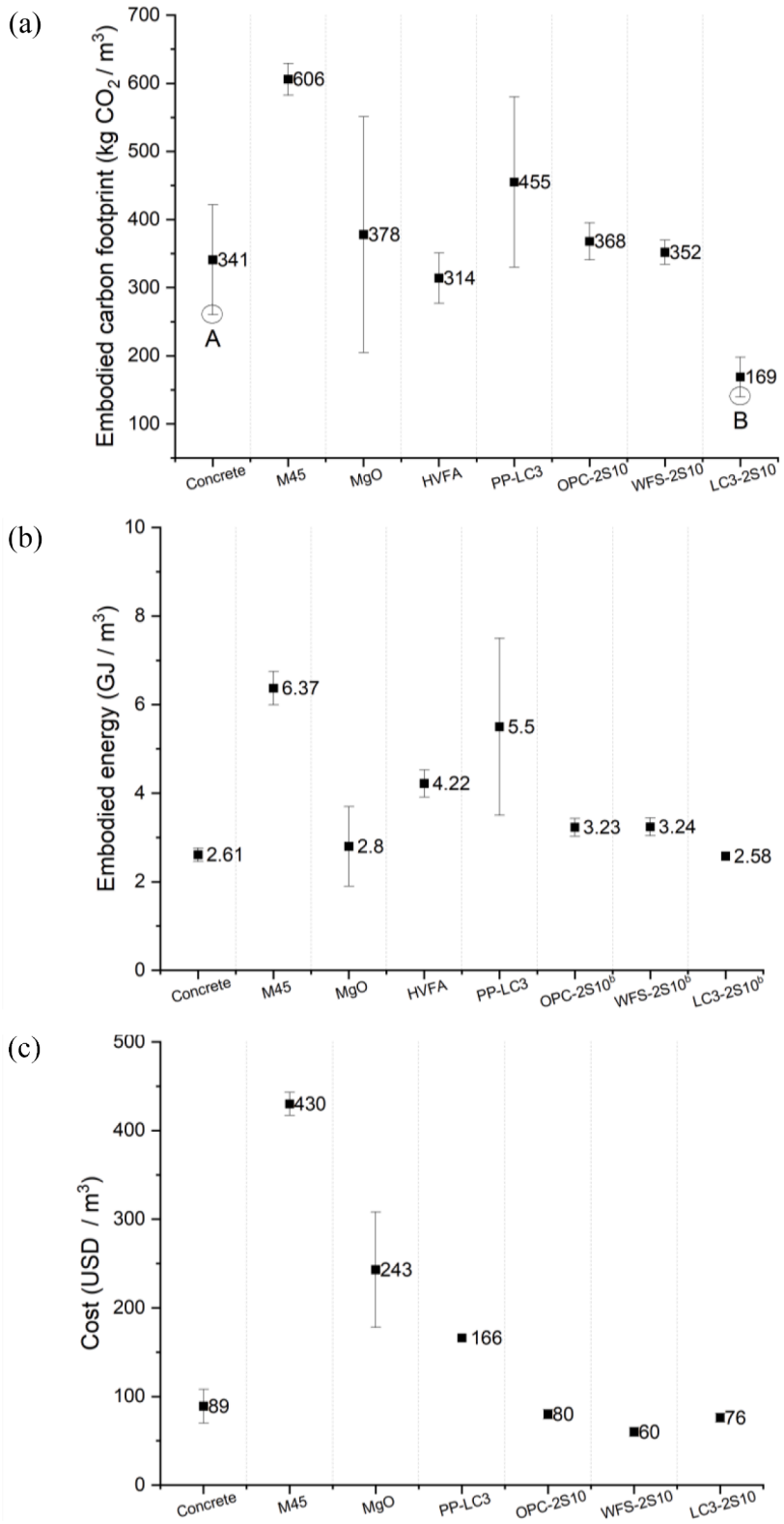

Fig. 4. The (a) embodied carbon footprint, (b) material embodied energy, and (c) material costs of conventional concrete, OPC-2S10, LC3–2S10, WFS-2S10, and other common ECC (Shoji et al., 2022).

and carbonation efficiency, four different amounts of sisal fiber were considered for both carbonation curing and air curing conditions for OPC-ECC. For the one with the best performance, OPC was substituted by LC3 or WFS to minimize the cost and embodied carbon footprint. Thermogravimetric analysis (TGA) was used to evaluate the CO_2 uptake of ECC mix proportions. Single fiber pull-out tests were conducted on WPE and Sisal fiber to determine the interfacial bond between the fiber and cementitious matrix.

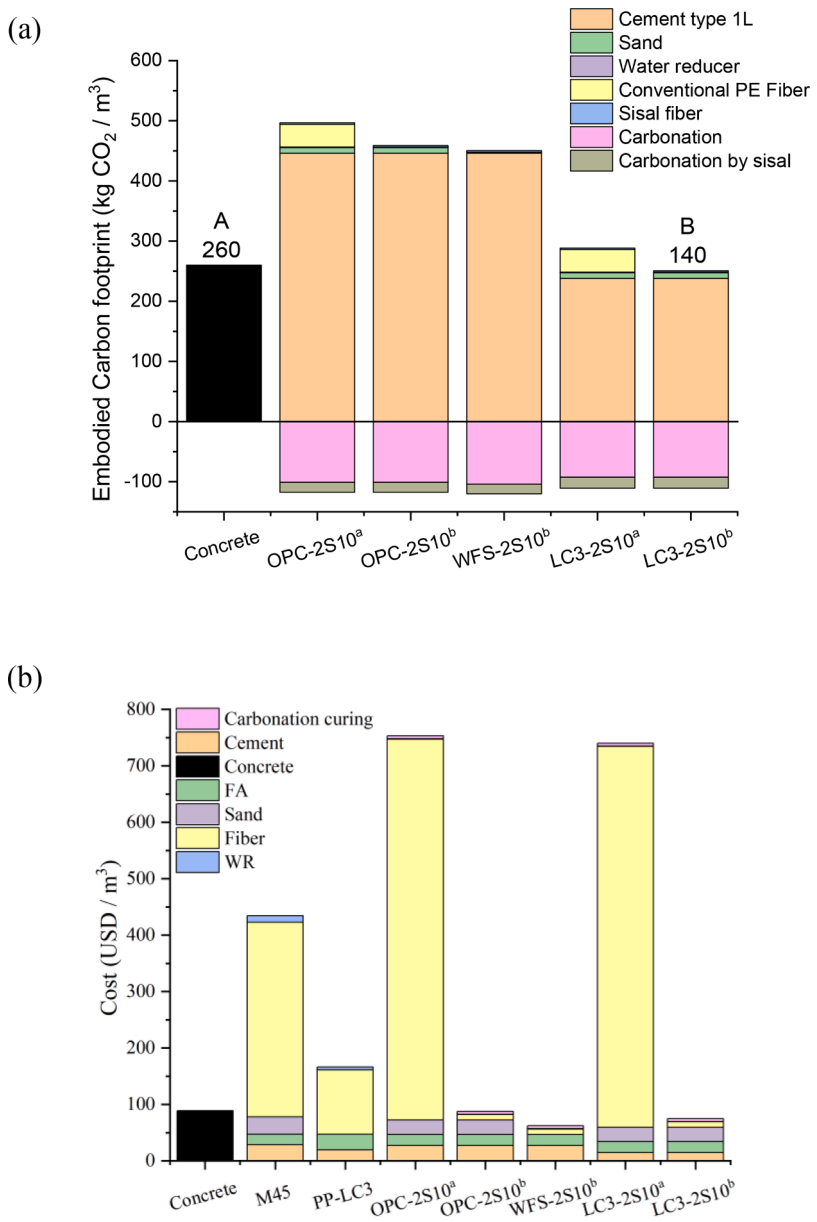

Fig. 5. Contributions of (a) embodied carbon footprint and (b) costs by ingredients of OPC-2S10[ab], LC3–2S10[ab], and WFS-2S10[b]. [a] with conventional PE fiber, [b] with WPE.

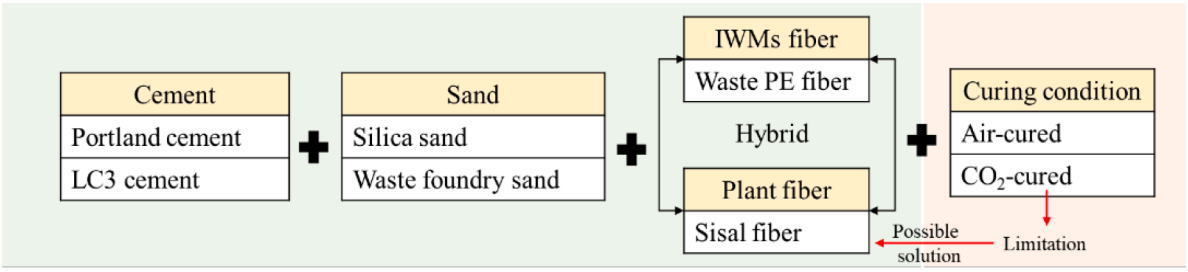

Fig. A1. Research framework for sustainable low-carbon ECC development.

2. Experimental program

2.1. Materials and mix proportions

Seven mix proportions were designed (Appendix A, Table A1). The materials for these mixtures include type 1 L ordinary Portland cement (OPC) from Lafarge Holcim cement, metakaolin (MK, Sikacrete®M-100) from Sika Corporation, limestone (LS, Snowhite®12-PT) from Omya Canada Inc., F-75 whole-grain silica sand from U.S. Silica Holdings Inc., waste foundry sand (WFS) with 270 μm mean particle size from Aero

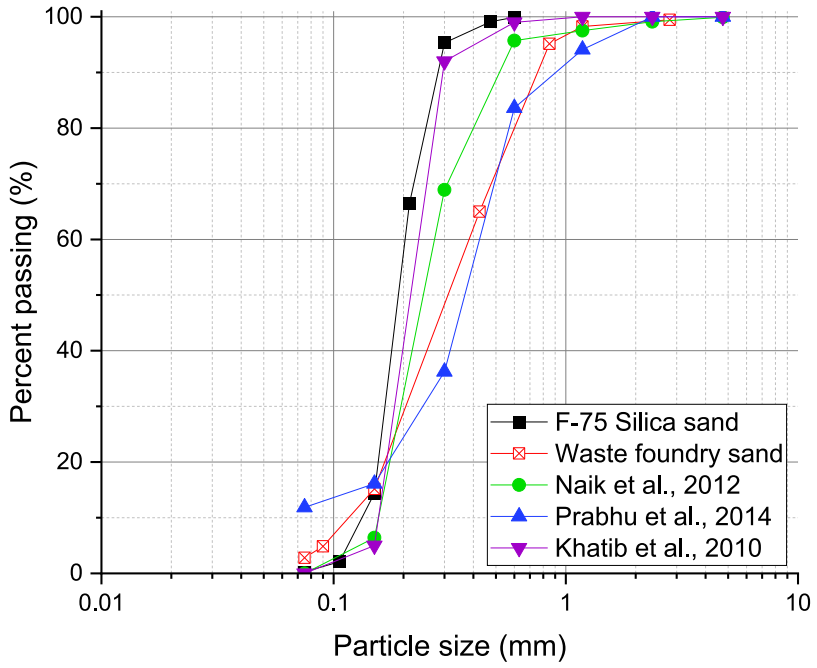

Fig. A2. Particle size distribution for F-75 silica sand and WFS (Ganesh Prabhu et al., 2015; Khatib et al., 2010; Naik et al., 2012).

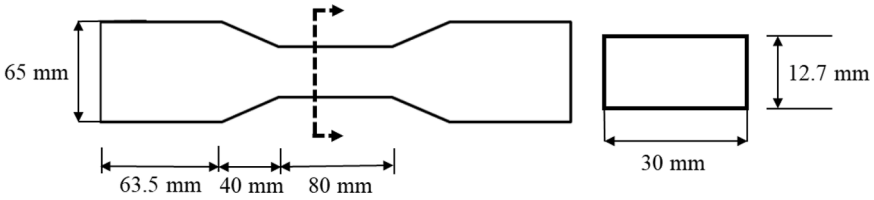

Fig. A3. Dimension of the dogbone-shape specimens for the uniaxial tension test.

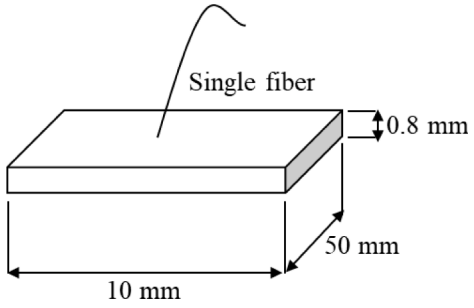

Fig. A4. Dimension of single fiber pull-out specimens.

Metals Inc., Class F fly ash (FA) from Boral Material Technologies Inc. The high-range water reducer (WR, MasterGlenium 7920) from BASF. The particle size distribution for silica sand and WFS was measured according to ASTM C136 (ASTM, 2022a) corresponding distribution curves for WFS from the literature (Ganesh Prabhu et al., 2015; Khatib et al., 2010; Naik et al., 2012) are also shown (Appendix A, Fig. A2). The chemical compositions of FA, MK, and LS are listed in Appendix A, Table A2.

The waste polyethylene rope fiber (WPE) is from discarded fishing gears, cut into 12 mm length filaments by laser. The sisal fiber is from Carriage House Paper. More detailed dimension and mechanical characteristics of WPE and sisal fiber can be found in Appendix A, Table A3.

2.2. Sample preparation and CO_2 curing process

Dogbone-shape specimens (Appendix A, Fig. A3) were cast for the uniaxial-tension test, the 50 × 50 × 50 mm^3 cubes for the compression test, and 305 × 76 × 38 mm^3 beams for the matrix toughness test. Single fiber pull-out specimens were also fabricated (Appendix A, Fig. A4). There were two curing conditions for each mix proportions: air curing of normal hydration process for non-carbonated reference and carbonation curing for carbonated specimens. All samples under both curing conditions were de-molded after 18 h until hardened. Air-cured specimens were cured in normal room conditions with 23±2 °C temperatures and 60 ± 5% relative humidity. Carbonation-cured specimens were subjected to 4 h fan drying process to remove the pore water in the mixtures to enhance the CO_2 diffusion (Zhang et al., 2016). Then, fan-dried specimens were cured under 5 bars bone dry CO_2 (99.8% purity) at room conditions (23±2 °C) for 24 h (Zhang et al., 2021). Additional cube specimens were cut to measure the carbonation depth and CO_2 uptake right after the carbonation-curing process, i.e., at the age of 48 h. The mechanical testing for all the other specimens, both air-cured and carbonation-cured, was conducted at 7 days and 28 days.

2.3. Test methods

2.3.1. Carbonation depth and CO_2 uptake

Phenolphthalein indicator was used to determine the carbonation depth for the carbonation-cured samples. The specimens were saw-cut after carbonation, and the phenolphthalein solution was sprayed to measure the uncolored thickness as carbonation depth.

CO_2 uptake was measured from specimens' mass loss during the

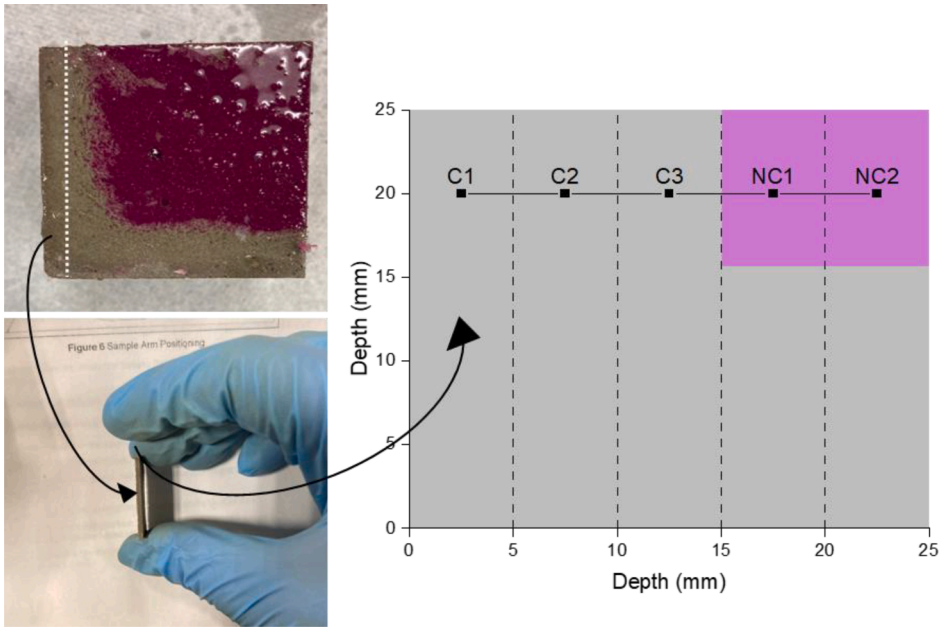

Fig. A5. Typical sample preparation of TGA for CO_2 uptake estimation.

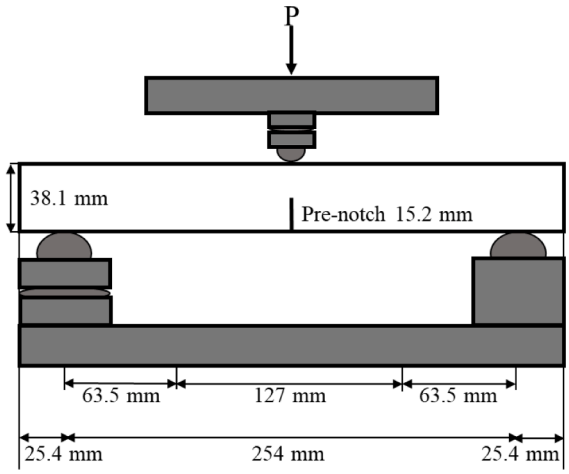

Fig. A6. Matrix toughness test setup.

decarbonation process of heating, i.e., TGA. The cube specimens were sliced into 5 mm thick layers and ground into powder. TGA was conducted from room temperature to 1100 °C. The decomposition temperature for calcite ($CaCO_3$) ranges from 550 to 950 °C (Karunadasa et al., 2019; Mentes et al., 2022; Valverde et al., 2015). Hence, the mass difference between 550 and 950 °C is the mass loss from the release of CO_2 and can be calculated using Eq. (1) (Zhang et al., 2021). Each 5 mm thick piece was measured, and the CO_2 uptake per cement mass throughout the cross-section can be obtained, as shown in Appendix A, Fig. A5.

$$CO_2\ \text{uptake}(\%) = \frac{(m_{550} - m_{950}) - (M_{550} - M_{950})}{m_{cement}} \times 100\% \quad (1)$$

where m_{550} and m_{950} are the masses of carbonation-cured samples at 550 and 950 °C, M_{550} and M_{950} are the masses of air-cured samples at 550 and 950 °C, and m_{cement} is the mass of the cement sample. Besides the CO_2 uptake estimation, to investigate the effect of introducing sisal fiber into the mixture, water loss during the enforced drying process was also considered and can be estimated by Eq. (2):

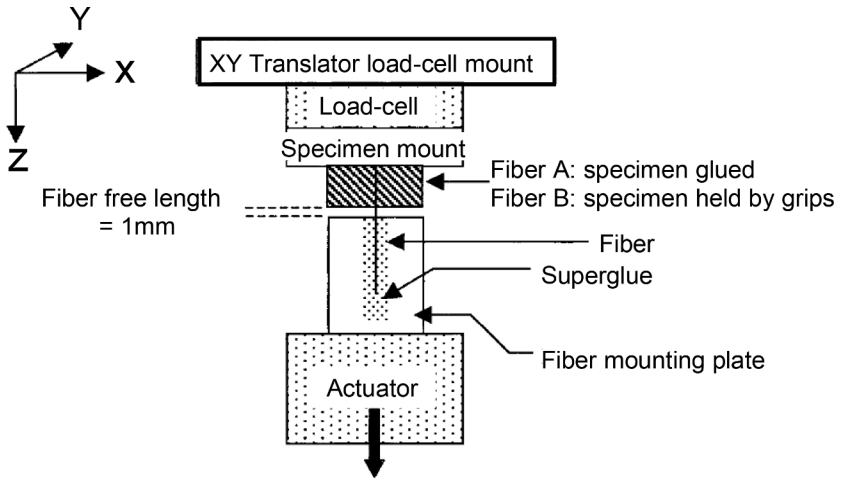

Fig. A7. Single fiber pull-out test setup (Redon et al., 2001).

Table A1
Mix proportion of ECC (kg/m^3).

Mixture	OPC	LS	MK	Sand		FA	Water	Fiber[a]		WR
				Silica sand	WFS			WPE	Sisal	
OPC-0S20	570	0	0	400	0	760	367.2	0%	2%	0.5
OPC-2S00	570	0	0	400	0	760	367.2	2%	0%	0.5
OPC-2S05	570	0	0	400	0	760	367.2	2%	0.5%	0.5
OPC-2S10	570	0	0	400	0	760	367.2	2%	1%	0.5
OPC-2S15	570	0	0	400	0	760	367.2	2%	1.5%	0.5
LC3–2S10 [b]	313.5	171	85.5	400	0	760	367.2	2%	1%	0.5
WFS-2S10	570	0	0	200	162.3	760	367.2	2%	1%	1.0

[a] Volume fraction.
[b] 55% OPC, 30% MK, and 15% LS for LC3 binder (Zhu et al., 2020).

Table A2
Chemical compositions of FA, MK, and LS (%).

Material	SiO_2	Al_2O_3	Fe_2O_3	CaO	K_2O	SO_3	MgO	TiO_2	P_2O_5	$CaCO_3$
FA	52.2	22.2	13.5	3.4	2.6	2.2	0.9	1.0	0.1	0.0
MK	50.8	46.6	0.5	0.0	0.3	0.1	0.0	1.7	0.0	0.0
LS	2.3	0.0	0.0	0.0	0.0	0.0	0.0	0.0	0.0	97.7

Table A3
Properties of fiber.

Fiber type	Length (mm)	Diameter (μm)	Fiber aspect ratio	Tensile strength (MPa)	Young's modulus (GPa)	Density (g/cm^3)
WPE	12[a]	42[a]	285	1550[b]	100.3[b]	0.97[b]
Sisal fiber[c]	8	150	53	490	21.5	1.45

[a] Measured by optical microscope.
[b] Measured according to ASTM 3822 and ASTM D3800 (ASTM, 2022c, 2020b).
[c] Provided by manufacturer.

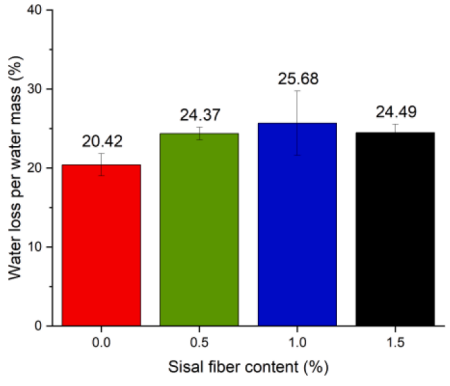

Fig. B1. Water loss for OPC-WPE-sisal fiber ECC by mass loss.

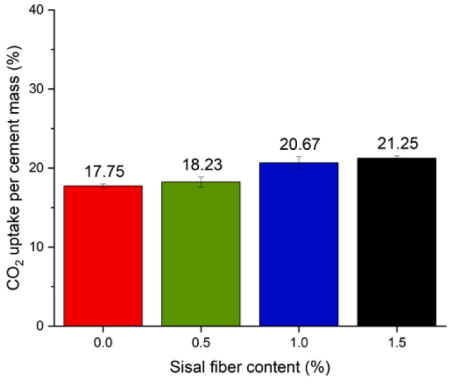

Fig. B2. CO_2 uptake per cement mass for OPC-WPE-Sisal fiber ECC by TGA.

$$\text{Water loss}(\%) = \frac{m_w - m_d}{m_{cement}} \times 100\% \quad (2)$$

where m_w and m_d are the masses of samples before and after 4 h drying process.

2.3.2. Mechanical tests

Uniaxial tension test and compression test were conducted after 7 days and 28 days of curing. A 100 KN capacity Material Testing Systems (MTS) loading frame was used for the uniaxial tension test in this study. Dogbone specimens were loaded under displacement control at a rate of 0.5 mm/min following JSCE (Yokota et al., 2008). Two linear variable displacement transducers (LVDT) were placed on the samples with a gauge length of 80 mm. A Forney loading machine was used for the compression test. 50 × 50 × 50 mm^3 cubes were conducted with a 0.5 MPa/s loading rate according to ASTM C109 (ASTM, 2020a).

Matrix toughness (K_m) of the ECC matrix was measured following the ASTM E399 (ASTM, 2022b), with a pre-notch (notch to height ratio = 0.4, i.e., 15.2 mm in this study) 305 × 76 × 38 mm^3 beam specimen. The experiment was conducted under displacement control at a rate of 0.5 mm/min. Detailed matrix toughness test setup and dimensions are shown in Appendix A, Fig. A6.

2.3.3. Single fiber pull out test

An Instron Model 8000 test system with a 5 N load cell was used for the single fiber pull out test to evaluate the fiber/matrix bridging and interfacial bond between fibers and cementitious matrix. WPS/sisal fibers were glued on the steel plate, connected to the actuator, and pulled at a constant loading rate of 0.5 mm/min, as shown in Fig. A7 (Redon et al., 2001). The load-displacement curves for the single fiber, chemical debonding energy, G_d, frictional bond strength, τ_0, and slip-hardening coefficient β were determined following the method of Katz and Li (1996).

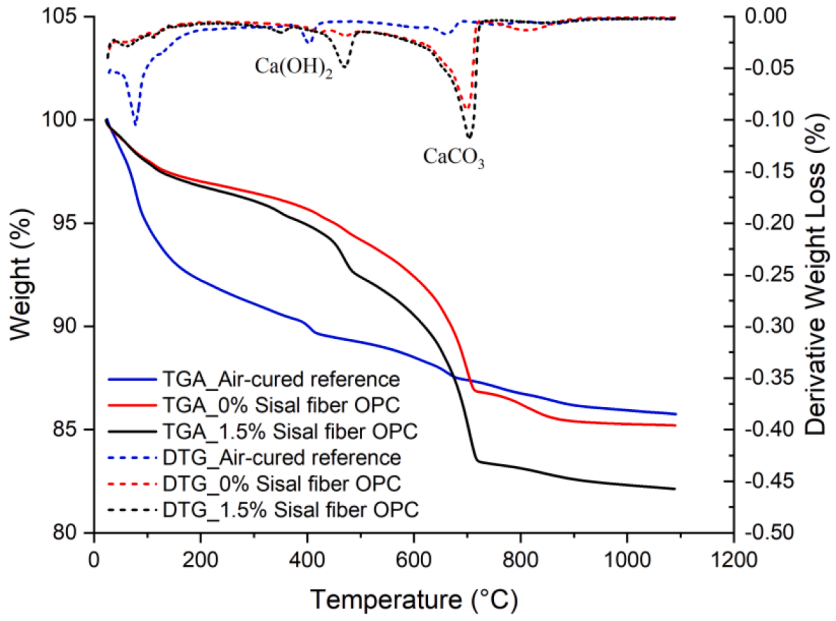

Fig. B3. Typical TGA & derivative thermogravimetry (DTG) for OPC-WPE-sisal fiber ECC.

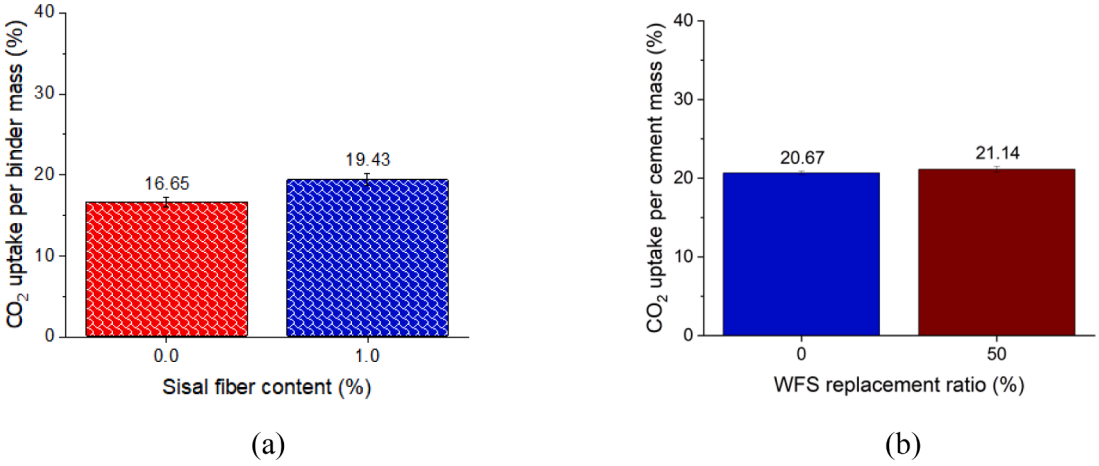

Fig. B4. CO_2 uptake for (a) LC3-WPE-sisal fiber ECC, (b) OPC-WPE-sisal fiber WFS ECC by TGA.

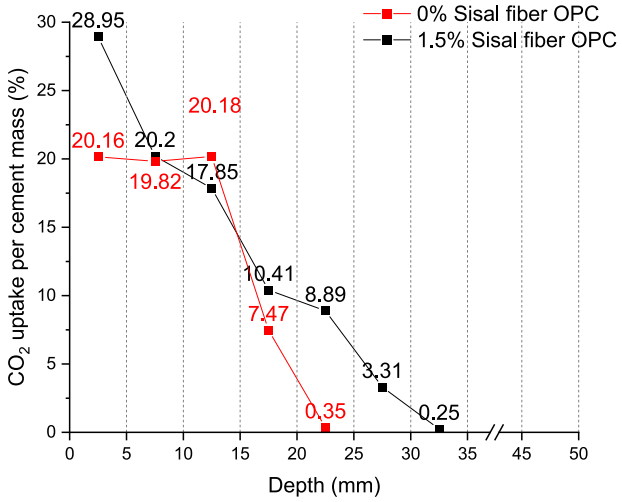

Fig. B5. CO_2 uptake for OPC-WPE-sisal fiber ECC among different depth.

2.3.4. *Pseudo-strain-hardening (PSH) indices from micromechanical modeling*

The fiber bridging capacity and complementary energy $J_b^{'}$ can be determined using fiber/matrix interfacial bond and matrix properties obtained from 0 as inputs based on the ECC micromechanical model Li, 2019; Yang et al., 2008). Then, PSH indices can be determined by Eq (3) and ((4), which can be used to evaluate the strain-hardening performance of ECC.

$$PSH_{energy} = \frac{J_b^{'}}{J_{tip}} \tag{3}$$

$$J_{tip} = \frac{K_m^2}{E_m} \tag{4}$$

where E_m is the Young's modulus of the matrix, and K_m is the matrix toughness. All units per parameter could be found in Appendix C, Table C1.

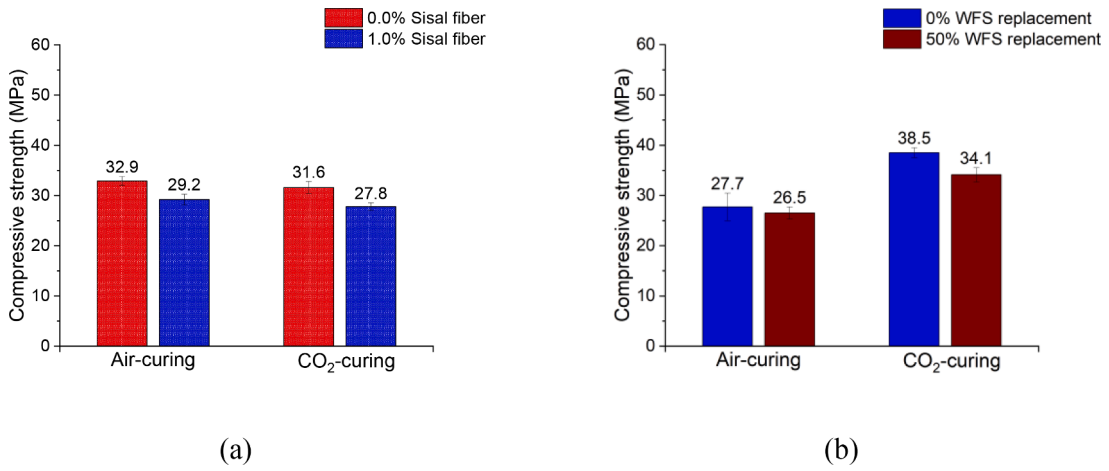

Fig. B6. Compressive strength of 1% sisal fiber (a) LC3-ECC, and (b) WFS-ECC.

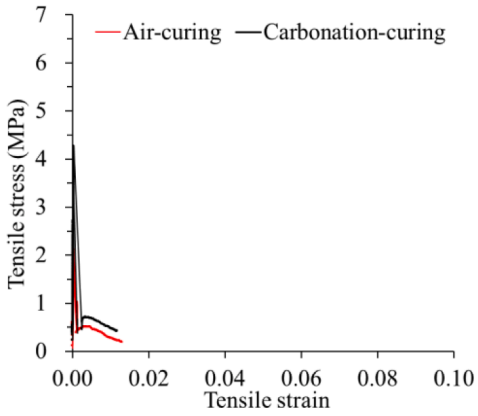

Fig. B7. Tensile stress-strain relationship for OPC-0S20, 0% WPE and 2% sisal fiber, ECC.

3. Results and discussion

3.1. Water loss and CO_2 uptake estimation

Sisal fibers serve as conduits for water and CO_2 during the enforced drying and carbonation curing process. Appendix B, Fig. B1 and Fig. B2 show the water loss and CO_2 uptake for the OPC cube specimens with sisal fiber content of 0.0% to 1.5%, i.e., OPC-2S00 to 2S15, for various sisal fiber contents. The average water loss without any sisal fiber is around 20.42%, and up to 25.68% for 1.0% of sisal fiber added (26% increase). The average CO_2 uptake (Fig. B2), obtained from the TGA curves (Fig. B3), increased from 17.75% to 18.23%, 20.67%, and 21.25% (3%, 16%, and 20% increase, respectively) when 0.5%, 1.0%, and 1.5% of sisal fiber were added. This finding validates the hypothesis that hollow sisal fiber can be effective as conduits for CO_2 penetration into the precast product during carbonation process. To further investigate the role of sisal fiber during carbonation curing, CO_2 uptake from the surface to core was measured for both air-cured and carbonation-cured samples (Appendix B, Fig. B5). There is a drastic decrease of CO_2 uptake when the depth exceeds 15 mm for the 0% sisal fiber sample, while the samples with sisal fibers can still maintain around 3.31% of CO_2 uptake at 25–30 mm depth. It is reasonable that there is an upper limit for CO_2 uptake for the 0% sisal fiber sample since the carbonation process is governed by the diffusion of CO_2 through the surface into the matrix (Monteiro et al., 2012; Possan et al., 2017). The formation of $CaCO_3$ during the carbonation process densifies the matrix, which makes it harder for CO_2 to further penetrate thorough the sample (Zhang et al., 2021). The tubular pillar geometry of sisal fiber channels the ingress of CO_2 through the densified cement matrix and lets CO_2 diffuse deeper, leading to a 16% increase of CO_2 uptake for 1.0% sisal fiber ECC. The carbonation patterns for the cross-section of the specimens, as revealed by the phenolphthalein indicator, also support this observation. As shown in Fig. 1(e) and (f), where the transparent color was observed between the interface of sisal fiber and cement matrix, indicating the formation of precipitates ($CaCO_3$) along the sisal fiber for the carbonation-cured specimens. With higher sisal fiber content, the transparent color area increases more (Fig. 1(f)). This phenomenon could not be found in the air-cured samples (see Fig. 1(b) and (c)).

Appendix B, Fig. B4(a) shows the CO_2 uptake for the LC3-ECC, i.e., LC3–2S10. The average CO_2 uptake increased from 16.25% to 19.43% (20% increase) when the sisal fiber content was increased from 0% to 1%. Also, Appendix B, Fig. B4(b) indicates the average CO_2 uptake for WFS-ECC, i.e., WFS-2S10, is comparable to normal silica sand ECC. The slightly increased CO_2 uptake from 20.67% to 21.14% (2% increase) may be caused by the larger particle size of the WFS, as shown in Appendix A, Fig. A2.

3.2. Micromechanical properties

3.2.1. Matrix properties

Appendix B, Table B1 illustrates the matrix properties for OPC-PE-sisal fiber ECC, including Young's modulus E_m and fracture toughness K_m. Carbonation curing increased E_m from 22.2 GPa to 25.8 GPa (16% increase). Carbonation curing makes the matrix stiffer by microstructural densification Šavija and Luković, 2016) through the $CaCO_3$ precipitation. A similar densification effect has been reported for conventional cement paste (B.Lecampion et al., 2011; Çopuroğlu and Schlangen, 2008) and ECC after carbonation curing (Zhang et al., 2021). In contrast, K_m diminished from 0.45 to 0.41 (9% reduction) for the carbonation-cured sample. The reduction suggests a slight increase in the brittleness of the matrix following carbonation curing. This matrix embrittlement effect is beneficial to enhancement of the PSH indices (see Eqs. (3) and ((4)).

3.2.2. Fiber/matrix interface

From a micromechanics-based viewpoint, excessively low resistance to fiber pull out and excessively high resistance that led to fiber rupture are the primary factors that limit the performance of ECC (Suthiwarapirak and Matsumoto, 2003; Zhang et al., 2001). Therefore, it is crucial to understand the effect of carbonation curing on the fiber/matrix interface properties.

Appendix B, Table B2 lists the WPE fiber/matrix interfacial bond, including chemical bond G_d, frictional bond τ_0, and slip hardening

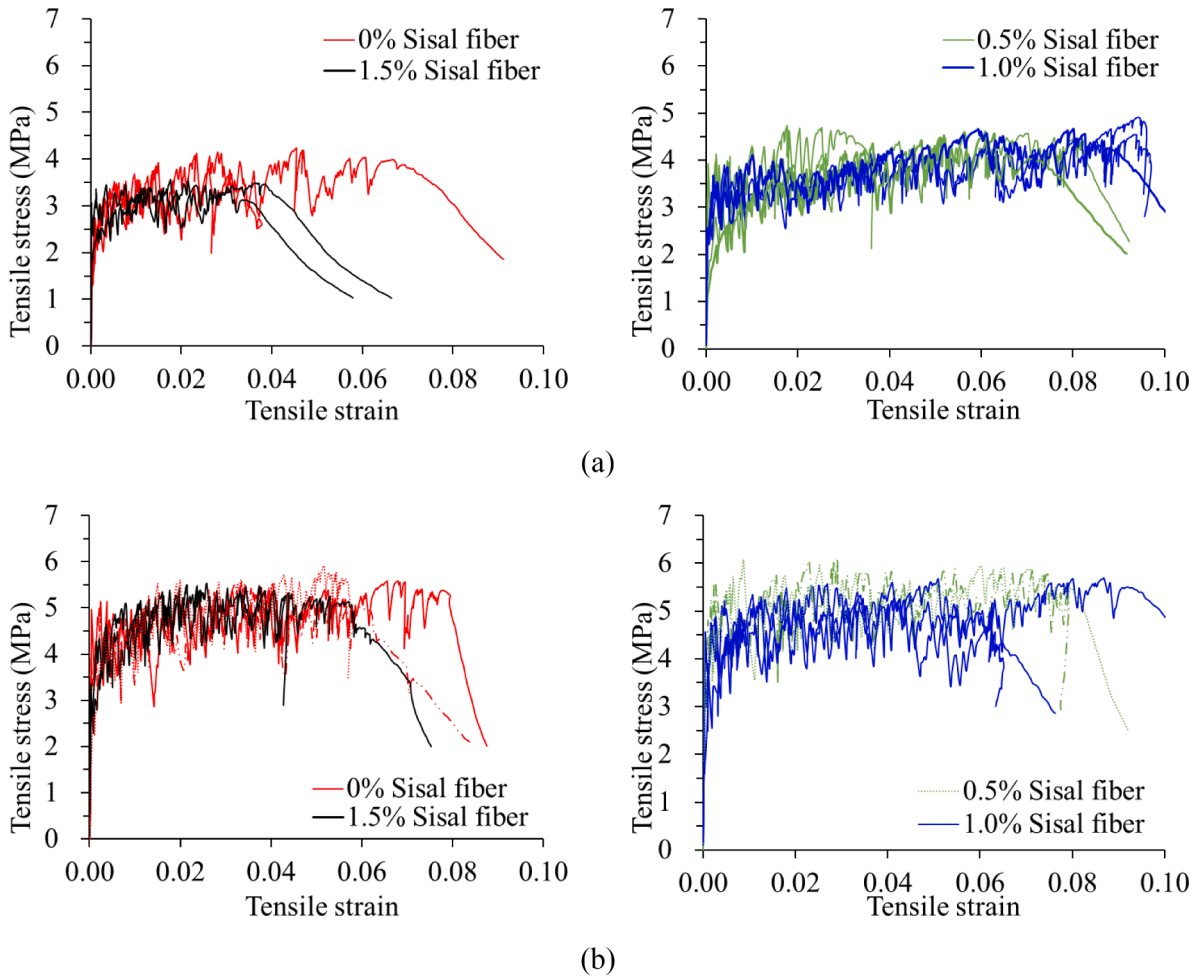

Fig. B8. Tensile stress-strain relationship for 2% WPE (a) air-cured, (b) CO_2-cured OPC-ECC at 7 days with different contents of sisal fiber.

coefficient β for air-cured and carbonation-cured ECC. Five single fiber pull-out specimens for each air-cured and carbonation-cured were measured. Carbonation curing increased the average G_d from 0.39 J/m^2 to 0.68 J/m^2 (74% increase) and the average τ_0 from 0.98 MPa to 1.45 MPa (48% increase), suggesting a more substantial fiber bridging capacity. The strengthening between fiber and matrix by carbonation curing makes the hydrophobic WPE fibers more resistant to debonding and pullout failure under tensile loading, leading to higher strength and ductility than air-cured ECC. The carbonation-induced increase of interfacial bond between fiber and matrix was also reported in a previous PVA ECC study (Zhang et al., 2021) and is attributed to the deposition of $CaCO_3$ along the fiber/matrix interface. Carbonation curing marginally increased β from 0.5 to 0.53 (6% increase), indicating the strain hardening process was not considerably influenced. In contrast, the average G_d and τ_0 increased from 0.01 to 0.05 J/m^2 and 0.49 to 0.92 MPa, respectively for sisal fiber/matrix interface (Appendix B, Table B3). Nevertheless, the interfacial bond after carbonation curing remained low. It can be anticipated that sisal fiber will encounter severe slippage and pull-out problems during tensile loading. This statement will be verified in later Section 3.3.2.

Strain hardening indices for both air-cured and carbonation-cured ECC are greater than 1 (Appendix B, Table B4), indicating that strain hardening criteria are satisfied for both curing conditions (Li, 2019). However, the PSH_{energy} decreased from 37.31 to 21.21 (43% decrease) after carbonation curing, which may lead to a reduced strain-hardening potential for ECC and need to be further confirmed.

3.3. Mechanical performance

3.3.1. Compressive strength

The compressive strength of the air-cured and carbonation-cured OPC-ECC are presented in Fig. 2. With increasing amount of sisal fiber from 0% to 1%, the compressive strength of the air-cured OPC-ECC decreased from 34.3 MPa to 27.7 MPa (19% decrease) at 7 days and from 44.3 MPa to 40.9 MPa (8% decrease) at 28 days due to the artificial flaws induced by adding the sisal fiber. Similarly, the compressive strength of the carbonation-cured ECC decreased when the sisal fiber was increased from 0% to 1%; from 38.9 MPa to 38.5 MPa (1% decrease) and 52.8 MPa to 47.6 MPa (10% decrease) at 7 days and 28 days, respectively. However, there is a significant compressive strength drop for 1.5% sisal fiber ECC (OPC-2S15). The compressive strength decreased from 38.9 MPa to 30.7 MPa (21% decrease) and 52.8 MPa to 36.4 MPa (31% decrease) at 7 days and 28 days. The high amount of fiber usage (2% WPE + 1.5% sisal fiber for a total 3.5% of volume fraction) led to the compressive strength reduction for 1.5% sisal fiber ECC, suggesting a problem with fiber dispersion difficulty.

Carbonation curing increased OPC-ECC's compressive strength from 34.3 MPa to 38.9 MPa (13% increase) for 0% sisal fiber added and 27.7 MPa to 38.5 MPa (39% increase) for 1% sisal fiber added at 7days. Similarly, the compressive strength increased from 44.3 MPa to 52.8 MPa (19% increase) and 40.9 MPa to 47.6 MPa (14%) for 0% and 1% sisal fiber ECC at 28 days. The increased compressive strength is due to the microstructural densification by the $CaCO_3$ precipitation for the carbonation-cured OPC-ECC. The strength gain by carbonation curing compensates for the strength loss by the addition of sisal fiber,

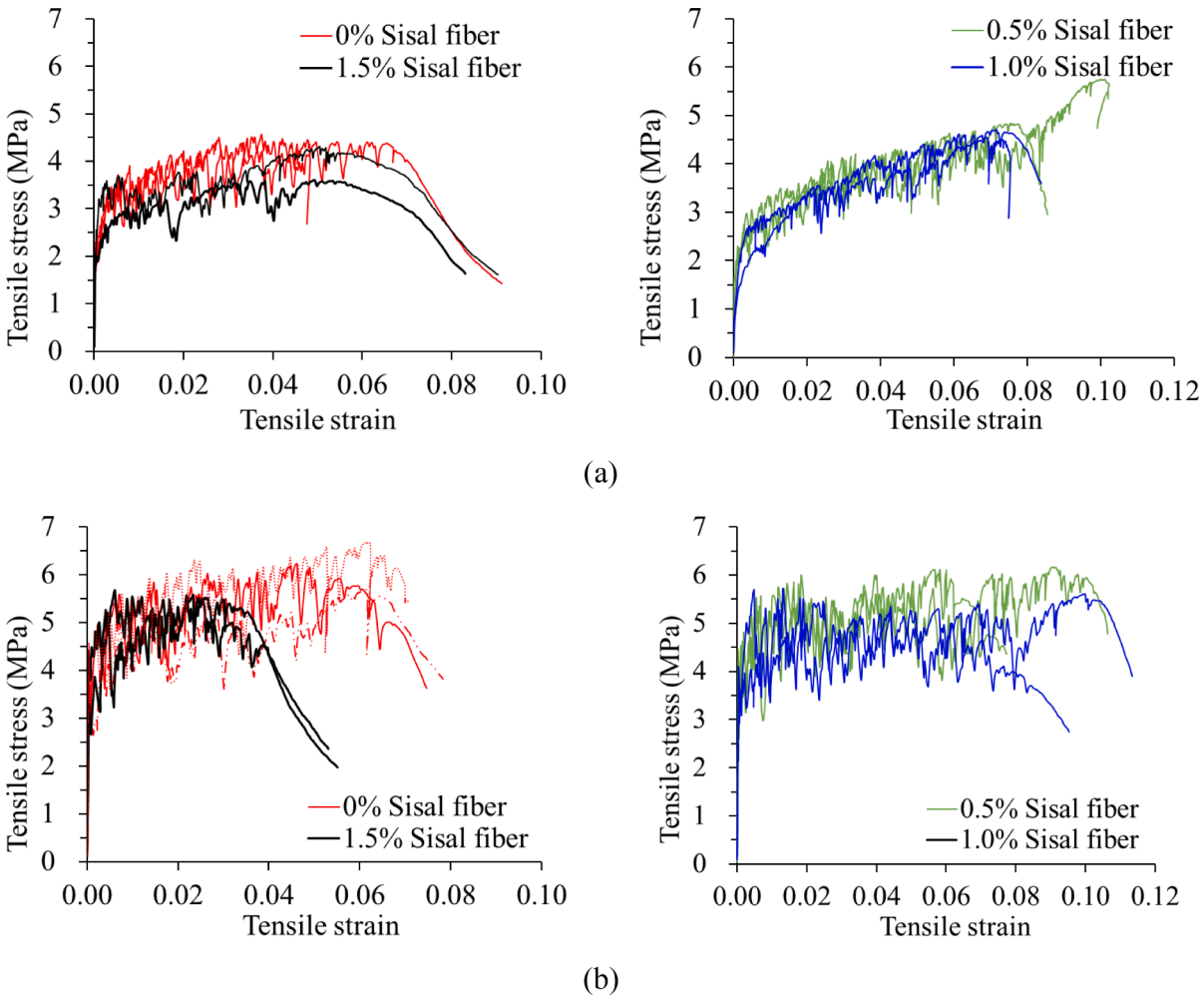

Fig. B9. Tensile stress-strain relationship for 2% WPE (a) air-cured, (b) CO_2-cured OPC-ECC at 28 days with different contents of sisal fiber.

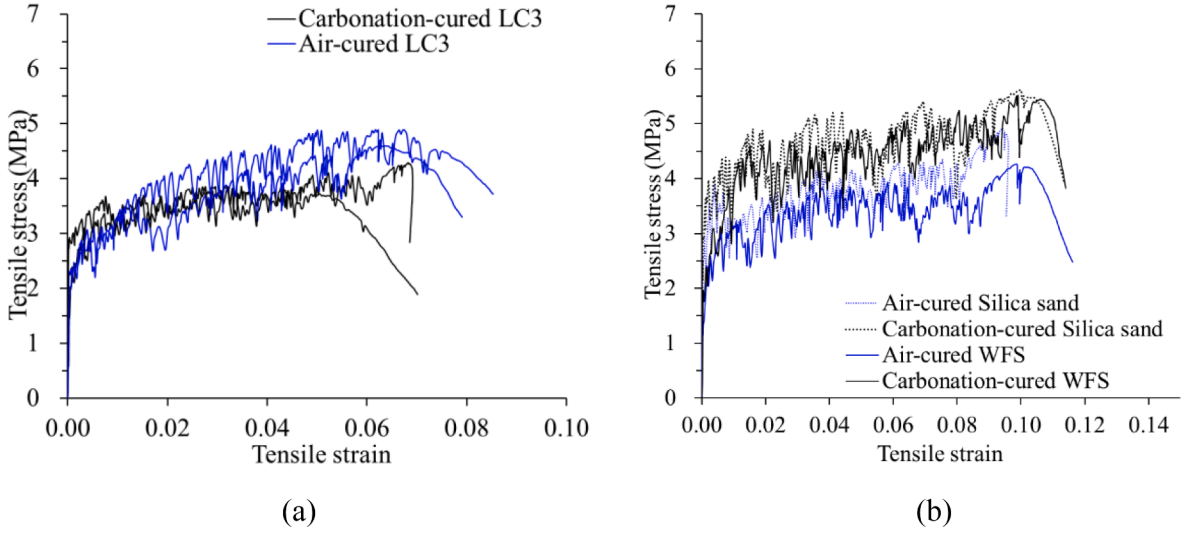

Fig. B10. Tensile stress-strain relationship for 1% sisal fiber (a) LC3-ECC, and (b) WFS-ECC.

suggesting a comparable compressive strength for carbonation-cured 1% sisal fiber to air-cured 0% sisal fiber OPC-ECC (47.6 MPa and 44.3 MPa).

Distinct from the strength gain of OPC-ECC after carbonation curing, the compressive strength of carbonation-cured LC3-ECC slightly decreased, as shown in Appendix B, Fig. B6 (a) from 32.9 MPa to 31.6 MPa (4% decrease). This could be attributed to the lower OPC content in addition to the calcium hydroxide (CH) competition between carbonation curing and the pozzolanic effect of MK for LC3 (comprising 55% OPC, 30% MK, 30% LS) (Antoni et al., 2012). Even without carbonation

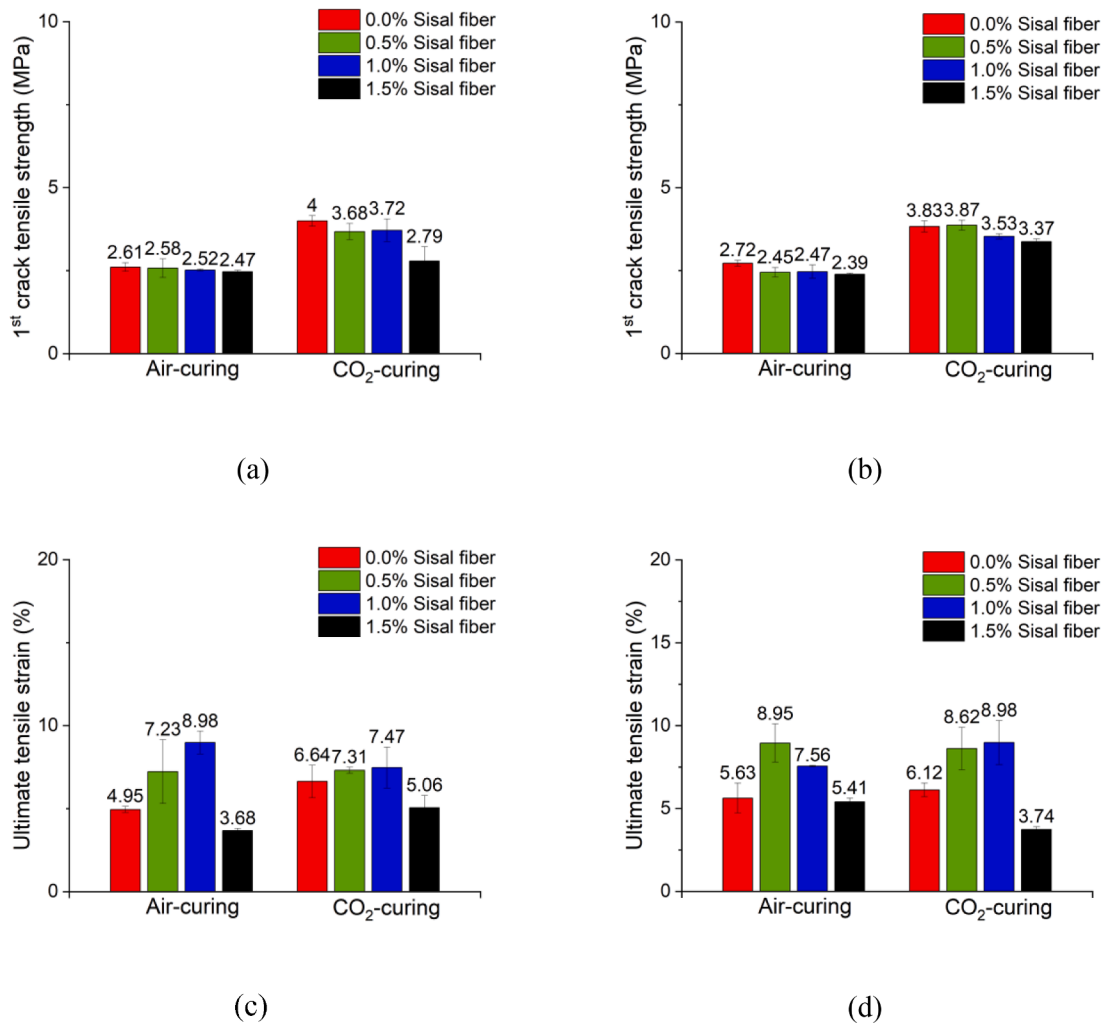

Fig. B11. Average first crack tensile strength at (a) 7 days, and (b) 28 days; Average tensile strain at (c) 7days, and (d) 28 days for 2% WPE OPC-ECC.

Fig. B12. Representative crack patterns for OPC-0S20, 0% WPE and 2% sisal fiber, ECC under ultimate tensile strain.

curing, LC3 consumes nearly all of CH after 3 days of hydration (Zhang et al., 2020a) Meanwhile, carbonation curing requires CH to react with CO_2, leading to lesser CH content and resulting in a lack of pozzolanic effect. Fig. B6(b) shows that compressive strength decreased for WFS-ECC, which is caused by the larger particle size and impurities intrinsic in WFS (Bhardwaj and Kumar, 2017; FHWA, 2008).

3.3.2. *Tensile performance*

Appendix B, Fig. B7 shows the tensile stress-strain curves for 0% WPE with 2% sisal fiber ECC, i.e., OPC-0S20. There is no strain-hardening behavior, and the specimen fails with a single crack. All sisal fibers were pulled out rather than ruptured during the tensile test, indicating low interfacial bond between the sisal fiber and the matrix, consistent with the results in Section 3.2.2.

The representative tensile stress-strain relationships for OPC-ECC are shown in Fig. 3, and the more detailed curves are shown in Appendix B, Fig. B8 and Fig. B9. The key tensile parameters, including average first crack strength, average ultimate strength, and average tensile strain, are summarized in Appendix B, Table B5 and Table B6. The 1st crack strength of OPC-ECC decreased with the increase of sisal fiber content due to the sisal fiber-induced artificial defects. Specifically, the 1% sisal fiber OPC-ECC reduced the 1st crack strength of 0% sisal fiber OPC-ECC from 2.61 MPa to 2.52 MPa (3% decrease), 4.00 MPa to 3.72 MPa (7% decrease) for air-cured and carbonation-cured samples at 7 days, respectively. The reduction of 1st crack strength benefits the multiple crack initiation, leading to more multiple crack formations and higher ultimate tensile strain by 81% increase and 13% increase for air-cured and carbonation-cured OPC-ECC. However, when the content of sisal fiber exceeded 1%, i.e., 1.5% of sisal fiber, the ultimate tensile strain decreased drastically from 8.98% to 3.68% (59% decrease) for air-cured and 7.47% to 5.06% (32% decrease) for carbonation-cured, as a result of

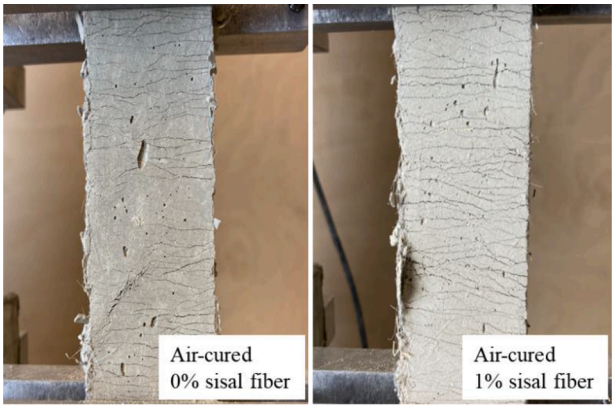

Fig. B13. Representative crack patterns for 0% and 1% sisal fiber of (a) air-cured and (b) carbonation-cured OPC-ECC under ultimate tensile strain.

poor fiber dispersion.

Carbonation curing increased the 1st crack strength of the specimens due to the densification of the matrix, which impeded the crack initiation and reduced the tensile ductility of ECC. However, as shown in Section 3.2.2, the fiber/matrix interfacial bond increased significantly after carbonation curing, i.e., 74% for G_d and 48% for τ_0, compensating for the disadvantage of 1st crack strength gain after carbonation curing. Therefore, the average ultimate strain was still enhanced for carbonation-cured 1% sisal fiber OPC-ECC by 13% and 47% at 7 and 28 days. The maximum strength also increased by 17%. The improved tensile performance of carbonation-cured ECC is consistent with the results in (Zhang et al., 2021, 2020a). The addition of sisal fiber and carbonation curing results in a tradeoff of artificial flaws, increased interfacial bond, and fiber dispersion.

In contrast, carbonation curing decreased the ultimate strength and tensile strain of LC3-ECC (Appendix B, Fig. B10 (a)). The lack of pozzolanic effect due to the competition of CH in the early ages of hydration during the carbonation curing process led to the ultimate strength decrease. The average ultimate strength and strain for 1% sisal fiber LC3-ECC still exceeded 3.98 MPa and 6.05%, showing a promising tensile performance comparable to previous LC3-ECC studied (Zhang et al., 2020a; Zhu et al., 2020). Appendix B, Fig. B10 (b) presents the similar ultimate strength and increased tensile strain of WFS-ECC

Table B1
Matrix properties for OPC-PE-sisal fiber ECC.

Curing condition	E_m (GPa)	K_m (MPa$\sqrt{m}$)
Air-cured	22.2 ± 1.31	0.45 ± 0.01
Carbonation-cured	25.8 ± 0.72	0.41 ± 0.01

Table B2
PE fiber/matrix interfacial bond for carbonation-cured and air-cured ECC.

Curing condition	Chemical bond G_d (J/m^2)	Frictional bond τ_0 (MPa)	Slip hardening coefficient β
Air-cured	0.39 ± 0.16	0.98 ± 0.20	0.50 ± 0.09
Carbonation-cured	0.68 ± 0.14	1.45 ± 0.26	0.53 ± 0.22

Table B3
Sisal fiber/matrix interfacial bond for carbonation-cured and air-cured ECC.

Curing condition	Chemical bond G_d (J/m^2)	Frictional bond τ_0 (MPa)
Air-cured	0.01 ± 0.00	0.49 ± 0.14
Carbonation-cured	0.05 ± 0.04	0.92 ± 0.11

Table B4
Strain-hardening indices for OPC-ECC.

Curing condition	J_b'(J/m^2)	J_{tip} (J/m^2)	PSH_{energy}
Air-cured	340.33 ± 28.7	9.12 ± 0.77	37.31 ± 6.32
Carbonation-cured	138.19 ± 24.7	6.52 ± 0.41	21.21 ± 5.13

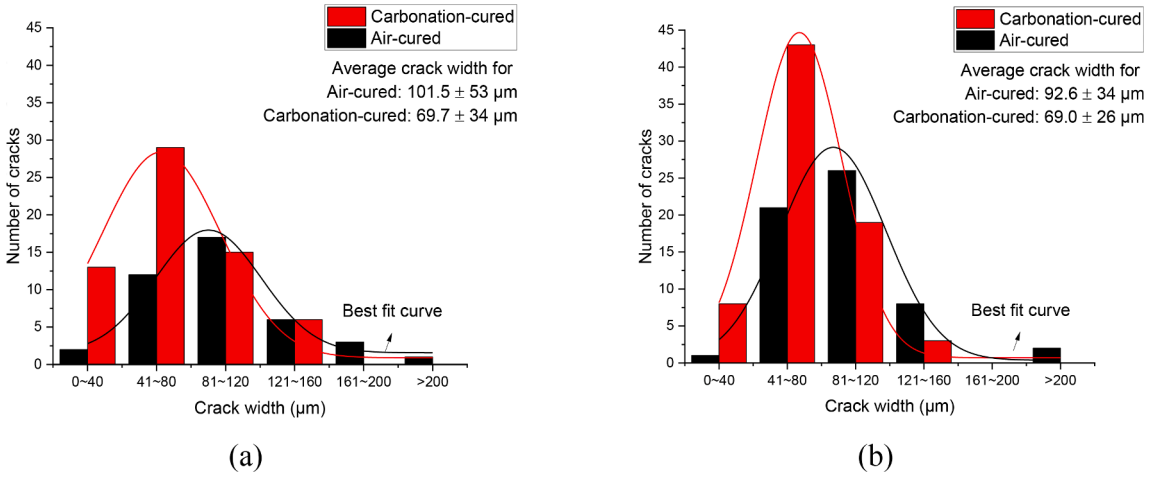

Fig. B14. Crack width distribution for 1% sisal fiber carbonation-cured and air-cured OPC-ECC with (a) silica sand and (b) WFS.

Table B5
Tensile properties of OPC-ECC at 7 days.

Sisal fiber content	Curing condition	Average 1st crack strength	Average ultimate strength	Average ultimate strain
0%	Air-cured	2.61 ± 0.13	4.03 ± 0.17	4.95 ± 0.19%
0.5%		2.58 ± 0.28	4.63 ± 0.08	7.23 ± 1.92%
1.0%		2.52 ± 0.03	4.71 ± 0.15	8.98 ± 0.68%
1.5%		2.47 ± 0.04	3.47 ± 0.02	3.68 ± 0.12%
0%	Carbonation-cured	4.00 ± 0.16	5.69 ± 0.16	6.64 ± 0.98%
0.5%		3.68 ± 0.24	6.09 ± 0.26	7.31 ± 0.18%
1.0%		3.72 ± 0.34	5.53 ± 0.19	7.47 ± 1.23%
1.5%		2.79 ± 0.43	5.45 ± 0.08	5.06 ± 0.73%

Table B6
Tensile properties of OPC-ECC at 28 days.

Sisal fiber content	Curing condition	Average 1st crack strength	Average ultimate strength	Average ultimate strain
0%	Air-cured	2.72 ± 0.09	4.48 ± 0.08	5.63 ± 0.90%
0.5%		2.45 ± 0.14	5.29 ± 0.46	8.95 ± 1.15%
1.0%		2.47 ± 0.20	4.63 ± 0.08	7.56 ± 0.04%
1.5%		2.39 ± 0.03	3.96 ± 0.36	5.41 ± 0.22%
0%	Carbonation-cured	3.83 ± 0.17	6.19 ± 0.40	6.12 ± 0.41%
0.5%		3.87 ± 0.15	6.14 ± 0.02	8.62 ± 1.28%
1.0%		3.53 ± 0.08	5.72 ± 0.02	8.98 ± 1.33%
1.5%		3.37 ± 0.09	5.62 ± 0.05	3.74 ± 0.17%

Table C1
Units of parameter.

Parameter	Symbol	Units
Masses of carbonation-cured samples at 550 °C	m_{550}	g
Masses of carbonation-cured samples at 950 °C	m_{950}	g
Mass of the cement sample	m_{cement}	g
Masses of samples before 4 h drying process	m_w	g
Masses of samples after 4 h drying process	m_d	g
Young's modulus	E_m	GPa
Matrix toughness	K_m	MPa$\sqrt{m}$
Chemical bond	G_d	J/m^2
Frictional bond	τ_0	MPa
Fiber bridging capacity and complementary energy	J_b'	J/m^2

compared to silica sand ECC. The ultimate strain for air-cured and carbonation-cured 1% sisal fiber WFS-ECC is 9.95% and 10.73%, respectively, exceeding 8.98% and 7.47% of strain for silica sand ECC (Appendix B, Fig. B11).

3.4. Crack patterns and crack width distribution

The 0% WPE 2% sisal fiber sample, i.e., OPC-0S20, shows only one localized failure crack, as shown in Appendix B, Fig. B12. Appendix B, Fig. B13 shows the representative crack patterns for 0% and 1% sisal fiber OPC-ECC under both curing conditions at failure. All OPC-ECC with 2%WPE present multiple cracks irrespective of the contents of sisal fiber. Adding more sisal fiber contributed to more crack numbers at failure with comparable crack width, suggesting the benefits of adding sisal fiber that enhance the ECC's tensile ductility.

Carbonation curing also improved the crack control capacity of ECC. Appendix B, Fig. B14 presents the crack width distribution for 1% sisal fiber carbonation-cured and air-cured OPC-ECC with silica sand and WFS. Carbonation curing leads to more crack formations and smaller crack width. The average cracks width for 1% sisal OPC-ECC and WPS-ECC decreased from 101.5 μm to 69.7 μm (31% decrease) and 92.6 μm to 69.0 μm (25% decrease), respectively. More tiny cracks below 80 μm were observed and there were no cracks larger than 160 μm for carbonation-cured specimens.

3.5. Sustainability of WPE-sisal fiber ECC

To evaluate the sustainability of the ECC, the embodied energy, embodied carbon footprint, and material costs, representing the total energy consumption, CO_2 emission, and costs during the manufacturing process of the materials, were assessed as Material Sustainability Indicators (MSIs) (Lepech et al., 2008). Table 1 lists the MSIs, including all the major ingredients for producing ECC. It should be noted that the material cost may fluctuate. The OPC type 1 L used in this study results in up to 10% reduction in carbon footprint compared to OPC type 1 listed in Table 1. According to Michigan Concrete Association and literature (Chung et al., 2021). The fly ash, WPE, and WFS in this study were assumed to be industrial waste streams with a net zero embodied energy consumption and CO_2 footprint.

Conventional concrete, typical M45-ECC, MgO-based ECC, high volume fly ash (HVFA) ECC, and LC3-PP-ECC were used as a benchmark to evaluate the MSIs of low-carbon ECC in this study as shown in Figs. 4 and 5, which also illustrates the CO_2 analysis for each ingredient based on the lower bounds of the variation, i.e., symbol A and symbol B in Fig. 5 represents the lower bounds of embodied carbon footprint of traditional concrete and LC3–2S10 in Fig. 4, respectively. By carbonation-curing and replacing conventional PE fiber by WPE, the embodied energy and carbon footprint (3.23 GJ/m^3 and 368 kg CO_2/m^3) of OPC-2S10 were found to decrease compared to M45-ECC (6.37 GJ/m^3 and 606 kg CO_2/m^3), while still higher than concrete (2.61 GJ/m^3 and 341 kg CO_2/m^3). Further replacing the OPC with LC3, i.e., LC3–2S10, significantly lowered the embodied CO_2 footprint for ECC. The average embodied CO_2 footprint of LC3–2S10 decreased to 169 kg CO_2/m^3 compared to concrete (341 kg CO_2/m^3) and M45-ECC (606 kg CO_2/m^3) with a 50% and 72% reduction, respectively, since cement contributed to the primary CO_2 emissions of ECC. The costs of LC3–2S10 and OPC-2S10 decreased to 76 and 80 USD/m^3 compared to M45-ECC (430 USD/m^3) since the main costs of ECC is from fiber (see Fig. 5), i.e., PVA fiber in M45 (345 USD/m^3) and PP fiber in LC3-PP mixture (115 USD/m^3). Substituting conventional PE (675 USD/m^3) with WPE reduces the fiber cost drastically to 9.6 USD/m^3, leading LC3–2S10 and OPC-2S10 ECC (76 and 80 USD/m^3 respectively) to be competitive with traditional concrete (89 USD/m^3). The costs of WFS-2S10 further decreased to 60 USD/m^3, which is 33% lower than traditional concrete. However, the embodied energy and carbon footprint of WFS-2S10 remained higher than concrete.

Taking the pavements construction as an example, among the total of 2.9 million miles of paved road in U.S., about 5% is paved with concrete (U.S. Department of Transportation Federal Highway Administration, 2020) consuming 22 million tons of concrete pavements (National Asphalt Pavement Association, 2020). If all concrete pavements were replaced with LC3-ECC in this study, the consumption of the WPE is 0.2 million tons, which is about 10% of annual ALDFG waste. Meanwhile, the embodied carbon footprint and costs will remain comparable with the conventional concrete and contribute to mitigating the environmental and economic impacts caused by marine waste. However, it should be noted that this WPE-sisal fiber ECC is only applicable to pre-cast pavements for which carbonation curing is suitable.

4. Conclusions

A sustainable low-carbon ECC is developed using industrial waste, renewable plant fiber, and carbonation curing. The repurposed materials include waste high modulus polyethylene (WPE) fiber from the marine industry and waste foundry sand. The developed carbonation-cured WPE-sisal fiber ECC has lower embodied energy, carbon, and cost than concrete and other grades of ECC while maintaining the unique high tensile ductility of the ECC family of composite materials. Meanwhile, the repurposing of WPE also serves as a potential solution for reducing marine plastic waste.

Specifically, the embodied carbon of the developed ECC was found to

reduce up to 50% that of traditional concrete with the incorporation of low-carbon LC3 binder, CO_2 sequestration, and waste polyethylene fiber and waste foundry sand utilization. Additionally, the cost of this ECC is only 67% that of traditional concrete. The resulting low-carbon ECC has a compressive strength of at least 30 MPa and the tensile strength of 4 MPa with a 6% tensile ductility. Furthermore, the developed ECC exhibits improved autogenous crack width control with an average crack width of 69 μm.

The addition of sisal fiber in the low carbon ECC was found to serve multiple purposes. From a sustainability point of view, renewable sisal fiber was found to enhance carbon sequestration by 10% by serving as conduits allowing deeper diffusion transport of CO_2 into the precast element during carbonation curing. From a mechanical performance point of view, sisal fibers were found to enhance the tensile ductility of the ECC by serving as artificial flaws and triggering a larger number of microcracks in the composite during tensile strain-hardening.

The developed ECC offers compelling advantages of low carbon footprint, cost-effectiveness, and ductile performance, thus positioning it as a competitive alternative to conventional concrete in both economic, environmental and technical performance terms.

This research opens a feasible pathway of creating civil infrastructure that has low embodied carbon in the material production phase as well as low operational carbon in the infrastructure use phase. Future research is needed to quantify the cost and carbon footprint savings in the life cycle of civil infrastructure using such low carbon ECC materials.

CRediT authorship contribution statement

Wei-Hsiu Hu: Conceptualization, Methodology, Investigation, Formal analysis, Writing – original draft, Writing – review & editing.

Duo Zhang, Esayas Ftwi: Investigation, Writing – review & editing.

Victor C. Li, Brian R. Ellis: Funding acquisition, Project administration, Conceptualization, Writing – review & editing.

Declaration of Competing Interest

The authors declare that they have no known competing financial interests or personal relationships that could have appeared to influence the work reported in this paper.

Acknowledgements

This research is supported by funding from the Center for Low Carbon Built Environment at the University of Michigan. Materials supplied by Holcim (OPC), Aero metals (WFS), Honeywell (WPE), and BASF (WR) are also gratefully acknowledged.

Appendix A. Detailed experimental program

Appendix B. Mechanical performances, crack patterns and carbonation efficiency of WPE-sisal fiber ECC

Appendix C. Units per parameter

References

Ahmad, J., Majdi, A., Deifalla, A.F., Kahla, N.B., Mohammed, A., 2022. Concrete reinforced with sisal fibers (SSF): overview of mechanical and physical properties. Crystals 12. https://doi.org/10.3390/cryst12070952.

Antoni, M., Rossen, J., Martirena, F., Scrivener, K., 2012. Cement substitution by a combination of metakaolin and limestone. Cem. Concr. Res. 42, 1579–1589. https://doi.org/10.1016/j.cemconres.2012.09.006.

ASTM, 2020a. Standard Test Method for Compressive Strength of Hydraulic Cement Mortars (Using 2-in. Or [50-mm] Cube Specimens). ASTM. https://doi.org/10.1520/C0109_C0109M-20.

ASTM, 2020b. Standard Test Method for Tensile Properties of Single Textile Fibers. ASTM. https://doi.org/10.1520/D3822_D3822M-14R20.

ASTM, 2022a. Standard Test Method for Sieve Analysis of Fine and Coarse Aggregates. ASTM. https://doi.org/10.1520/C0136_C0136M-19.

ASTM, 2022b. Standard Test Method for Linear-Elastic Plane-Strain Fracture Toughness of Metallic Materials. ASTM. https://doi.org/10.1520/E0399-22.

ASTM, 2022c. Standard Test Method for Density of High-Modulus Fibers. ASTM. https://doi.org/10.1520/D3800-22.

Bahraq, A.A., Maslehuddin, M., Al-Dulaijan, S.U., 2020. Macro- and micro-properties of engineered cementitious composites (ECCs) incorporating industrial waste materials: a review. Arab. J. Sci. Eng. 45, 7869–7895. https://doi.org/10.1007/s13369-020-04729-7.

Beaumont, N.J., Aanesen, M., Austen, M.C., Börger, T., Clark, J.R., Cole, M., Hooper, T., Lindeque, P.K., Pascoe, C., Wyles, K.J., 2019. Global ecological, social and economic impacts of marine plastic. Mar. Pollut. Bull. 142, 189–195. https://doi.org/10.1016/j.marpolbul.2019.03.022.

Bhardwaj, B., Kumar, P., 2017. Waste foundry sand in concrete: a review. Constr. Build. Mater. 156, 661–674. https://doi.org/10.1016/j.conbuildmat.2017.09.010.

Borrelle, S.B., Ringma, J., Law, K.L., Monnahan, C.C., Lebreton, L., Mcgivern, A., Murphy, E., Jambeck, J., Leonard, G.H., Hilleary, M.A., Eriksen, M., Possingham, H. P., de Frond, H., Gerber, L.R., Polidoro, B., Tahir, A., Bernard, M., Mallos, N., Barnes, M., Rochman, C.M., 2020. Predicted growth in plastic waste exceeds efforts to mitigate plastic pollution. Science (1979) 369, 1515–1518.

Broeren, M.L.M., Dellaert, S.N.C., Cok, B., Patel, M.K., Worrell, E., Shen, L., 2017. Life cycle assessment of sisal fibre – exploring how local practices can influence environmental performance. J. Clean. Prod. 149, 818–827. https://doi.org/10.1016/j.jclepro.2017.02.073.

Camargo, M.M., Adefrs Taye, E., Roether, J.A., Redda, D.T., Boccaccini, A.R., 2020. A review on natural fiber-reinforced geopolymer and cement-based composites. Materials. https://doi.org/10.3390/ma13204603.

Cancio Díaz, Y., Sánchez Berriel, S., Heierli, U., Favier, A.R., Sánchez Machado, I.R., Scrivener, K.L., Martirena Hernández, J.F., Habert, G., 2017. Limestone calcined clay cement as a low-carbon solution to meet expanding cement demand in emerging economies. Dev. Eng. 2, 82–91. https://doi.org/10.1016/j.deveng.2017.06.001.

Chung, H.W., Subgranon, T., Tia, M., Deford, H., Armenteros, J., 2021. The effects of reduced paste volume in Portland limestone cement concrete. Mag. Concr. Res. 73, 958–972. https://doi.org/10.1680/jmacr.19.00541.

Çopuroğlu, O., Schlangen, E., 2008. Modeling of frost salt scaling. Cem. Concr. Res. 38, 27–39. https://doi.org/10.1016/j.cemconres.2007.09.003.

Damtoft, J.S., Lukasik, J., Herfort, D., Sorrentino, D., Gartner, E.M., 2008. Sustainable development and climate change initiatives. Cem. Concr. Res. 38, 115–127. https://doi.org/10.1016/j.cemconres.2007.09.008.

FHWA, 2008. User guidelines for waste and byproduct materials in pavement construction. FHWA-RD-97-148 report.

Fu, C., Chen, M., Guo, R., Qi, R., 2022. Green-engineered cementitious composite production with high-strength synthetic fiber and aggregate replacement. Materials (Basel) 15. https://doi.org/10.3390/ma15093047.

Ganesh Prabhu, G., Bang, J.W., Lee, B.J., Hyun, J.H., Kim, Y.Y., 2015. Mechanical and durability properties of concrete made with used foundry sand as fine aggregate. Adv. Mater. Sci. Eng. 2015 https://doi.org/10.1155/2015/161753.

Global Ghost Gear Initiative, 2022. GGGI 2021 annual report.

Hasan, K., Islam, M.T., Tohfa, T.S., Yahaya, F.M., 2023. Using basalt fiber reinforced polymer as steel reinforcement -review. Construction 3, 40–53.

Hasanuddin, I., Mawardi, I., Nurdin, N., Jaya, R.P., 2023. Evaluation of properties of hybrid laminated composites with different fiber layers based on Coir/Al2O3 reinforced composites for structural application. Results Eng. 17, 100948 https://doi.org/10.1016/j.rineng.2023.100948.

Hu, W.H., Zhang, D., Ellis, B.R., Li, V.C., 2023. The impact of carbonation curing on the fatigue behavior of polyvinyl alcohol engineered cementitious composites (PVA-ECC). J. Adv. Concr. Technol. 21 (4) https://doi.org/10.3151/jact.21.322.

Karunadasa, K.S.P., Manoratne, C.H., Pitawala, H.M.T.G.A., Rajapakse, R.M.G., 2019. Thermal decomposition of calcium carbonate (calcite polymorph) as examined by in-situ high-temperature X-ray powder diffraction. J. Phys. Chem. Solids 134, 21–28. https://doi.org/10.1016/j.jpcs.2019.05.023.

Katz, A., Li, V.C., 1996. A special technique for determining the bond strength of micro-fibres in cement matrix by pullout test. J. Mater. Sci. Lett.

Khatib, J.M., Baig, S., Bougara, A., Booth, C., 2010. Foundry sand tilization in concrete production. In: 2nd International Conference on Sustainable Construction Materials and Technologies, pp. 931–935.

B. Lecampion, J. Vanzo, F.J. Ulm, B. Hue, C. Germa, I. Khalfallah, J. Dirrenberge, 2011. Evolution of Portland cement mechanical properties exposed to CO2 rich fluids: investigation at different scales. Mechanics and Physics of Porous Solids (MPPS) – A tribute to Prof. Olivier Coussy.

Lepech, M.D., Li, V.C., 2009. Water permeability of engineered cementitious composites. Cem Concr Compos 31, 744–753. https://doi.org/10.1016/j.cemconcomp.2009.07.002.

Lepech, M.D., Li, V.C., Robertson, R.E., Keoleian, G.A., 2008. Design of green engineered cementitious composites for improved sustainability. ACI Mater. J. 105, 567–575. https://doi.org/10.14359/20198.

Li, V.C., 2019. Engineered Cementitious Composites – Bendable Concrete For Sustainable and Resilient Infrastructure. published by Springer, Germany, p. 419. https://doi.org/10.1007/978-3-662-58438-5. ISBN 978-3-662-58437-8pp.
Li, V.C., Herbert, E.N., 2013. Self-healing of microcracks in engineered cementitious composites (ECC) under a natural environment. Materials (Basel) 6, 2831–2845. https://doi.org/10.3390/ma6072831.
Li, V.C., Wang, S., Wu, C., 2001. Tensile strain-hardening behavior or polyvinyl alcohol engineered cementitious composite (PVA-ECC). ACI Mater. J. 98, 483–492. https://doi.org/10.14359/10851.
Li, V.C., Wu, C., Wang, S., Ogawa, A., Saito, T., 2002. Interface tailoring for strain-hardening polyvinyl alcohol-engineered cementitious composite (PVA-ECC). ACI Mater. J. 99, 463–472.
Macfadyen, G.(Graeme), Huntington, T., Cappell, Rod., Food and Agriculture Organization of the United Nations., United Nations Environment Programme., 2009. Abandoned, lost or otherwise discarded fishing gear. United Nations Environment Programme.
Marceau, M.L., Nisbet, M.A., Vangeem, M.G., 2006. Life cycle inventory of Portland cement concrete.
Maria, I., Bertelsen, G., Ottosen, L.M., 2016. Engineering properties of fibres from waste fishing nets materials. Syst. Struct. Civil Eng. Circ. Ocean.
Mentes, D., Tóth, C.E., Nagy, G., Muránszky, G., Póliska, C., 2022. Investigation of gaseous and solid pollutants emitted from waste tire combustion at different temperatures. Waste Manag. 149, 302–312. https://doi.org/10.1016/j.wasman.2022.06.027.
Monteiro, I., Branco, F.A., Brito, J.de, Neves, R., 2012. Statistical analysis of the carbonation coefficient in open air concrete structures. Constr. Build. Mater. 29, 263–269. https://doi.org/10.1016/j.conbuildmat.2011.10.028.
Muthangya, M., Mshandete, A.M., Kivaisi, A.K., 2009. Two-stage fungal pre-treatment for improved biogas production from sisal leaf decortication residues. Int. J. Mol. Sci. 10, 4805–4815. https://doi.org/10.3390/ijms10114805.
Naik, T.R., Asce, F., Kraus, R.N., Ramme, B.W., Asce, M., Canpolat, F., 2012. Effects of fly ash and foundry sand on performance of architectural precast concrete. https://doi.org/10.1061/(ASCE).
National Asphalt Pavement Association, 2020. The asphalt pavement industry fast facts. https://doi.org/10.13140/RG.2.2.21946.82888.
Nguyen, N.M., Han, T.H., Park, J.K., Kim, J.J., 2021. Strength and toughness of waste fishing net fiber-reinforced concrete. Materials (Basel) 14.
Othman, R., Jaya, R.P., Duraisamy, Y., Sulaiman, M.A., Chong, B.W., Ghamari, A., 2023. Efficiency of waste as cement replacement in foamed concrete—a review. Sustainability 15, 5163. https://doi.org/10.3390/su15065163.
Pacheco-Torgal, F., Abdollahnejad, Z., Miraldo, S., Kheradmand, M., 2017. Alkali-Activated Cement-Based Binders (AACBs) As Durable and Cost-Competitive Low-CO2 Binder Materials: Some Shortcomings That Need to Be Addressed, in: Handbook of Low Carbon Concrete. Elsevier Inc., pp. 195–216. https://doi.org/10.1016/B978-0-12-804524-4.00009-9
Possan, E., Thomaz, W.A., Aleandri, G.A., Felix, E.F., dos Santos, A.C.P., 2017. CO2 uptake potential due to concrete carbonation: a case study. Case Stud. Construct. Mater. 6, 147–161. https://doi.org/10.1016/j.cscm.2017.01.007.
Redon, C., Li, V.C., Wu, C., Hoshiro, H., Saito, T., Ogawa, A., 2001. Measuring and modifying interface properties of PVA fibers in ECC matrix. J. Mater. Civil Eng. 13, 399–406. https://doi.org/10.1061/(asce)0899-1561(2001)13:6(399).
Ritchie, H. and Roser, M., 2018. Plastic pollution. Published online at OurWorldInData.org. https://ourworldindata.org/plastic-pollution.
Ritchie, H., Roser, M., Rosado, P., 2020. CO_2 and greenhouse gas emissions. Published online at OurWorldInData.org. https://ourworldindata.org/co2-and-other-greenhouse-gas-emissions.
Rostami, V., Shao, Y., Boyd, A.J., He, Z., 2012. Microstructure of cement paste subject to early carbonation curing. Cem. Concr. Res. 42, 186–193. https://doi.org/10.1016/j.cemconres.2011.09.010.
Sahmaran, M., Li, M., Li, V.C., 2007. Transport properties of engineered cementitious composites under chloride exposure. ACI Mater. J. 104, 604–611.
Sánchez Berriel, S., Favier, A., Rosa Domínguez, E., Sánchez MacHado, I.R., Heierli, U., Scrivener, K., Martirena Hernández, F., Habert, G., 2016. Assessing the environmental and economic potential of limestone calcined clay cement in Cuba. J. Clean. Prod. 124, 361–369. https://doi.org/10.1016/j.jclepro.2016.02.125.
Šavija, B., Luković, M., 2016. Carbonation of cement paste: understanding, challenges, and opportunities. Constr. Build. Mater. https://doi.org/10.1016/j.conbuildmat.2016.04.138.
Saxena, M., Pappu, A., Haque, R., Sharma, A., 2011. Sisal fiber based polymer composites and their applications. Cellulose Fibers: Bio- and Nano-Polymer Composites.
Shoji, D., He, Z., Zhang, D., Li, V.C., 2022. The greening of engineered cementitious composites (ECC): a review. Constr. Build. Mater. https://doi.org/10.1016/j.conbuildmat.2022.126701.
Suthiwarapirak, P., Matsumoto, T., 2003. Fiber bridging degradation based fatigue analysis of ECC under flexure. J. Appl. Mech. 6, 1179–1188. https://doi.org/10.2208/journalam.6.1179.
The PEW Charitable Trusts and SystemIQ, 2020. Breaking the plastic wave: a comprehensive assessment of pathways towards stopping ocean plastic pollution.
Thomas, B.C., Jose, Y.S., 2022. A study on characteristics of sisal fiber and its performance in fiber reinforced concrete. Mater. Today: Proceedings 51, 1238–1242. https://doi.org/10.1016/j.matpr.2021.07.312.
U.S. Department of Transportation Federal Highway Administration, 2020. Table HM-12 highway statistics 2020.
Valverde, J.M., Perejon, A., Medina, S., Perez-Maqueda, L.A., 2015. Thermal decomposition of dolomite under CO2: insights from TGA and in situ XRD analysis. Phys. Chem. Chem. Phys. 17, 30162–30176. https://doi.org/10.1039/c5cp05596b.
Wan Ibrahim, M.H., Jamaludin, N., Irwan, J.M., Ramadhansyah, P.J., Suraya, H.A., 2014. Compressive and flexural strength of foamed concrete containing polyolefin fibers. Adv. Mat. Res. 911, 489–493.
Wei, J., 2018. Degradation behavior and kinetics of sisal fiber in pore solutions of sustainable cementitious composite containing metakaolin. Polym. Degrad. Stab. 150, 1–12. https://doi.org/10.1016/j.polymdegradstab.2018.01.027.
Wei, J., Meyer, C., 2014. Improving degradation resistance of sisal fiber in concrete through fiber surface treatment. Appl. Surf. Sci. 289, 511–523. https://doi.org/10.1016/j.apsusc.2013.11.024.
Wu, H.L., Zhang, D., Ellis, B.R., Li, V.C., 2018. Development of reactive MgO-based engineered cementitious composite (ECC) through accelerated carbonation curing. Constr. Build. Mater. 191, 23–31. https://doi.org/10.1016/j.conbuildmat.2018.09.196.
Yang, E.H., Wang, S., Yang, Y., Li, V.C., 2008. Fiber-bridging constitutive law of engineered cementitious composites. J. Adv. Concr. Technol. 6, 181–193.
Yokota, H., Rokugo, K., Sakata, N., 2008. JSCE recommendations for design and construction of high performance fiber reinforced cement composite with multiple fine cracks.
Yu, J., Wu, H.L., Leung, C.K.Y., 2020. Feasibility of using ultrahigh-volume limestone-calcined clay blend to develop sustainable medium-strength engineered cementitious composites (ECC). J. Clean. Prod. 262 https://doi.org/10.1016/j.jclepro.2020.121343.
Yu, K.Q., Yu, J.T., Dai, J.G., Lu, Z.D., Shah, S.P., 2018. Development of ultra-high performance engineered cementitious composites using polyethylene (PE) fibers. Constr. Build. Mater. https://doi.org/10.1016/j.conbuildmat.2017.10.040.
Yu, K.Q., Zhu, W.J., Ding, Y., Lu, Z.D., Yu, J.tao, Xiao, J.Z., 2019. Micro-structural and mechanical properties of ultra-high performance engineered cementitious composites (UHP-ECC) incorporation of recycled fine powder (RFP). Cem. Concr. Res. 124, 105813 https://doi.org/10.1016/j.cemconres.2019.105813.
Zhang, D., Cai, X., Shao, Y., 2016. Carbonation curing of precast fly ash concrete. J. Mater. Civil Eng. 28, 04016127 https://doi.org/10.1061/(asce)mt.1943-5533.0001649.
Zhang, D., Ellis, B.R., Jaworska, B., Hu, W.H., Li, V.C., 2021. Carbonation curing for precast engineered cementitious composites. Constr. Build. Mater. 313 https://doi.org/10.1016/j.conbuildmat.2021.125502.
Zhang, D., Jaworska, B., Zhu, H., Dahlquist, K., Li, V.C., 2020a. Engineered cementitious composites (ECC) with limestone calcined clay cement (LC3). Cem. Concr. Compos. 114 https://doi.org/10.1016/j.cemconcomp.2020.103766.
Zhang, D., Liu, T., Shao, Y., 2020b. Weathering carbonation behavior of concrete subject to early-age carbonation curing. J. Mater. Civil Eng. 32, 04020038 https://doi.org/10.1061/(asce)mt.1943-5533.0003087.
Zhang, D., Shao, Y., 2016. Early age carbonation curing for precast reinforced concretes. Constr. Build. Mater. 113, 134–143. https://doi.org/10.1016/j.conbuildmat.2016.03.048.
Zhang, D., Yu, J., Wu, H., Jaworska, B., Ellis, B.R., Li, V.C., 2020c. Discontinuous micro-fibers as intrinsic reinforcement for ductile engineered cementitious composites (ECC). Compos. B Eng. https://doi.org/10.1016/j.compositesb.2020.107741.
Zhang, J., Stang, H., Li, V.C., 2001. Crack bridging model for fibre reinforced concrete under fatigue tension. Int. J. Fatigue 23, 655–670. https://doi.org/10.1016/S0142-1123(01)00041-X.
Zhou, S., Xie, L., Jia, Y., Wang, C., 2020. Review of cementitious composites containing polyethylene fibers as repairing materials. Polymers (Basel) 12 (11). https://doi.org/10.3390/polym12112624.
Zhu, H., Zhang, D., Wang, T., Wu, H., Li, V.C., 2020. Mechanical and self-healing behavior of low carbon engineered cementitious composites reinforced with PP-fibers. Constr. Build. Mater. 259, 119805 https://doi.org/10.1016/j.conbuildmat.2020.119805.